

Comparative carbon cycle dynamics of the present and last interglacial

Victor Brovkin, Tim Brücher, Thomas Kleinen, Sönke Zaehle, Fortunat Joos, Raphaël Roth, Renato Spahni, Jochen Schmitt, Hubertus Fischer, Markus Leuenberger, et al.

▶ **To cite this version:**

Victor Brovkin, Tim Brücher, Thomas Kleinen, Sönke Zaehle, Fortunat Joos, et al.. Comparative carbon cycle dynamics of the present and last interglacial. Quaternary Science Reviews, 2016, 137, pp.15-32. 10.1016/j.quascirev.2016.01.028 . insu-01352021

HAL Id: insu-01352021
https://insu.hal.science/insu-01352021

Submitted on 5 Mar 2021

HAL is a multi-disciplinary open access archive for the deposit and dissemination of scientific research documents, whether they are published or not. The documents may come from teaching and research institutions in France or abroad, or from public or private research centers.

L'archive ouverte pluridisciplinaire **HAL**, est destinée au dépôt et à la diffusion de documents scientifiques de niveau recherche, publiés ou non, émanant des établissements d'enseignement et de recherche français ou étrangers, des laboratoires publics ou privés.



Distributed under a Creative Commons Attribution - NoDerivatives 4.0 International License

Quaternary Science Reviews 137 (2016) 15–32

Contents lists available at ScienceDirect

Quaternary Science Reviews

journal homepage: www.elsevier.com/locate/quascirev

Comparative carbon cycle dynamics of the present and last interglacial

Victor Brovkin [a, *], Tim Brücher [a, 1], Thomas Kleinen [a], Sönke Zaehle [b], Fortunat Joos [c], Raphael Roth [c], Renato Spahni [c], Jochen Schmitt [c], Hubertus Fischer [c], Markus Leuenberger [c], Emma J. Stone [d], Andy Ridgwell [d], Jérôme Chappellaz [e, f], Natalie Kehrwald [g], Carlo Barbante [g], Thomas Blunier [h], Dorthe Dahl Jensen [h]

[a] Max Planck Institute for Meteorology, Hamburg, Germany
[b] Max Planck Institute for Biogeochemistry, Jena, Germany
[c] Climate and Environmental Physics, Physics Institute and Oeschger Centre for Climate Change Research, University of Bern, Bern, Switzerland
[d] BRIDGE, School of Geographical Sciences, University of Bristol, United Kingdom
[e] Univ. Grenoble Alpes, LGGE, F-38000, Grenoble, France
[f] CNRS, LGGE, F-38000, Grenoble, France
[g] Institute for the Dynamics of Environmental Processes-CNR, University of Venice, Italy
[h] University of Copenhagen, Denmark

ARTICLE INFO

Article history:
Received 25 June 2015
Received in revised form
24 January 2016
Accepted 28 January 2016
Available online 8 February 2016

Keywords:
Carbon cycle
Climate
Models
Interglacials
The Holocene
The Eemian
Peatland
Fire
Coral reef

ABSTRACT

Changes in temperature and carbon dioxide during glacial cycles recorded in Antarctic ice cores are tightly coupled. However, this relationship does not hold for interglacials. While climate cooled towards the end of both the last (Eemian) and present (Holocene) interglacials, CO_2 remained stable during the Eemian while rising in the Holocene. We identify and review twelve biogeochemical mechanisms of terrestrial (vegetation dynamics and CO_2 fertilization, land use, wildfire, accumulation of peat, changes in permafrost carbon, subaerial volcanic outgassing) and marine origin (changes in sea surface temperature, carbonate compensation to deglaciation and terrestrial biosphere regrowth, shallow-water carbonate sedimentation, changes in the soft tissue pump, and methane hydrates), which potentially may have contributed to the CO_2 dynamics during interglacials but which remain not well quantified. We use three Earth System Models (ESMs) of intermediate complexity to compare effects of selected mechanisms on the interglacial CO_2 and $\delta^{13}CO_2$ changes, focusing on those with substantial potential impacts: namely carbonate sedimentation in shallow waters, peat growth, and (in the case of the Holocene) human land use. A set of specified carbon cycle forcings could qualitatively explain atmospheric CO_2 dynamics from 8 ka BP to the pre-industrial. However, when applied to Eemian boundary conditions from 126 to 115 ka BP, the same set of forcings led to disagreement with the observed direction of CO_2 changes after 122 ka BP. This failure to simulate late-Eemian CO_2 dynamics could be a result of the imposed forcings such as prescribed $CaCO_3$ accumulation and/or an incorrect response of simulated terrestrial carbon to the surface cooling at the end of the interglacial. These experiments also reveal that key natural processes of interglacial CO_2 dynamics – shallow water $CaCO_3$ accumulation, peat and permafrost carbon dynamics - are not well represented in the current ESMs. Global-scale modeling of these long-term carbon cycle components started only in the last decade, and uncertainty in parameterization of these mechanisms is a main limitation in the successful modeling of interglacial CO_2 dynamics.

© 2016 The Authors. Published by Elsevier Ltd. This is an open access article under the CC BY license (http://creativecommons.org/licenses/by/4.0/).

1. Introduction

A number of uncertainties complicate future projections of atmospheric CO_2 concentration and climate change (Ciais et al., 2013). In conjunction with the development of mechanistic models of the climate system and carbon cycle, the starting point to addressing these uncertainties is to understand the relationship

* Corresponding author. MPI for Meteorology, Bundesstr. 53, 20146, Hamburg, Germany.
E-mail address: victor.brovkin@mpimet.mpg.de (V. Brovkin).
[1] Now at GEOMAR Helmholtz Centre for Ocean Research, Kiel, Germany.

http://dx.doi.org/10.1016/j.quascirev.2016.01.028
0277-3791/© 2016 The Authors. Published by Elsevier Ltd. This is an open access article under the CC BY license (http://creativecommons.org/licenses/by/4.0/).

between surface temperatures and atmospheric CO_2 concentrations in the warm intervals of the recent past. The tight coupling between Antarctic temperature and CO_2 during glacial cycles has been known since pioneering studies of the Antarctic ice cores (Barnola et al., 1987; Neftel et al., 1982). Recent studies reveal past CO_2 dynamics during the present (Indermühle et al., 1999; Monnin et al., 2004) and last interglacial periods (Schneider et al., 2013) with much higher precision and accuracy. These analyses demonstrate that during the present interglacial (Holocene), atmospheric CO_2 increased by about 20 ppm from 7 ka BP to before the onset of the industrial era (Fig. 1). In the last interglacial period (Eemian), CO_2 varied around the level of about 270–280 ppm without any significant trend from 126 to 115 ka BP (Fig. 1). Since temperatures in Antarctica decreased towards the end of both periods, the temperature - CO_2 relationship common for the glacial cycles (Petit et al., 1999; van Nes et al., 2015) and, especially, deglaciations (Parrenin et al., 2013) is not valid for these two interglacials.

Here, we address the difference in the interglacial CO_2 dynamics using two approaches. First, we provide a review of proxy data and mechanisms of carbon cycle changes during the Holocene and Eemian. In section 2, we summarize the current state of knowledge with regards to CO_2 variability during interglacials, reviewing the various possible carbon cycle mechanisms that can affect atmospheric CO_2. This overview is followed by a summary of available proxy constraints on these processes. In the second part of the paper, we present model setup (section 3) and results (section 4) from factorial simulations using three Earth System Models of Intermediate Complexity (EMIC). For this model intercomparison, we focus on time periods starting thousands of years after the terminations in order to minimize the memory effects of carbon cycle reorganization during deglaciation. For the Holocene, we chose the period from 8 ka BP, when interglacial climate conditions were well established, to 0.5 ka BP excluding the fossil fuel effect on the carbon cycle. For the Eemian, we analyze the period from 126 to 115 ka BP which corresponds to the Marine Isotopic Stage 5e (Tzedakis et al., 2012). Finally, we summarize how the CO_2 and $\delta^{13}CO_2$ ice core records during both 8–0.5 and 126–115 ka BP periods can be quantified based on the previous research and results of our model intercomparison.

2. An overview of proxy data and mechanisms of interglacial CO_2 change

2.1. Insights from the ice core $\delta^{13}CO_2$ records

Discrimination of the heavy ^{13}C isotope during photosynthesis affects land-atmosphere carbon fluxes and modifies the $^{13}C/^{12}C$ ratio of atmospheric $^{13}CO_2$ (e.g., Lloyd and Farquhar, 1994). An increase (decrease) in organic carbon storage on land leads to higher (lower) $^{13}C/^{12}C$ ratios in the atmosphere. Stable carbon isotope records from the ice cores, expressed as a deviation from the Vienna PeeDee Belemnite (VPDB) reference value in permil (‰), $\delta^{13}CO_2$, could be used to attribute changes in CO_2 to different sources. Indermühle et al. (1999) used newly available $\delta^{13}CO_2$ data at that time to conduct the first attempt to constrain the sources responsible for the growing CO_2 trend in the Holocene. These authors reconstructed the Holocene CO_2 evolution in detail, but had to rely on low temporal resolution measurements of $\delta^{13}CO_2$ with larger

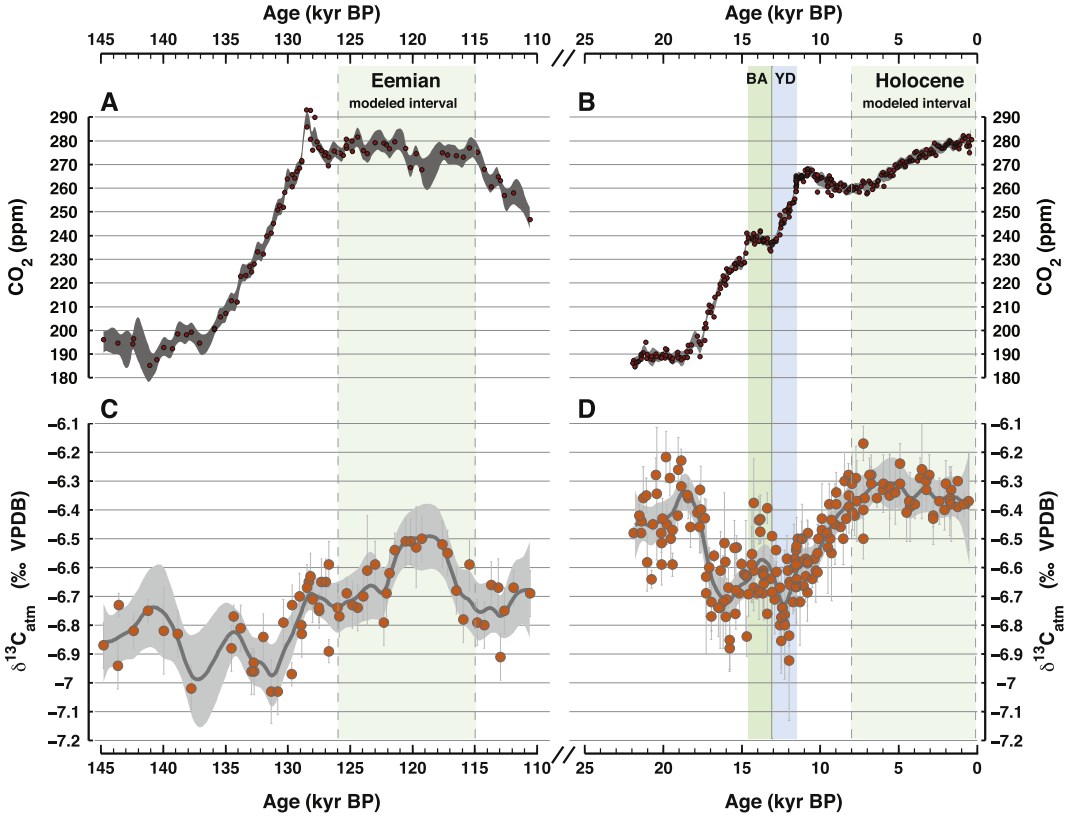


Fig. 1. Atmospheric CO_2 concentration, ppm (A, B) and $\delta^{13}CO_2$, ‰ (C, D) during the present (A, C) and the last (B, D) interglacial as reconstructed from Antarctic ice cores. For the Holocene, CO_2 data are from Monnin et al. (2004) and (Schmitt et al., 2012) plotted on top of a 1σ -error envelope using a Monte-Carlo approach with a cut-off period of 500 years; $\delta^{13}CO_2$ are the data as shown in (Schmitt et al., 2012) along the 1σ-error envelope (cut-off 2000 years). For the Eemian, CO_2 data are from (Lourantou et al., 2010; Schneider et al., 2013) plotted on top of a 1σ-error envelope and cut-off of 800 years, and $\delta^{13}CO_2$ data are from (Schneider et al., 2013) with a cut-off period of 3000 years.

uncertainty than achieved in recent approaches. They deconvolved the budget equations of CO_2 and $\delta^{13}CO_2$ for the unknown oceanic and terrestrial carbon sources and sinks while invoking processes such as changes in land carbon storage, changes in Sea Surface Temperatures (SST) and changes in the calcium carbonate cycle to explain their records. This pioneering work started a search for comprehensive, process-based explanations of Holocene CO_2 forcings.

Elsig et al. (2009) presented a new high-precision and high-resolution $\delta^{13}CO_2$ record (Fig. 1) that provided for the first time a reliable and strong top-down constraint on the Holocene CO_2 changes. These authors repeated the deconvolution of the CO_2 and $\delta^{13}CO_2$ records and suggested that the 20 ppm increase of atmospheric CO_2 and the small decrease in $\delta^{13}CO_2$ of about 0.05‰ during the late Holocene are mainly be explained by contributions from pre-Holocene memory effects, such as carbonate compensation of earlier land-biosphere uptake, and coral reef formation, with only a minor contribution from a small decrease in the land-biosphere carbon inventory. In quantitative terms, their deconvolution of the CO_2 and $\delta^{13}CO_2$ records yields a land carbon uptake of ca. 60 GtC from 7 to 5 ka BP, followed by a cumulative land carbon release of 36 ± 37 GtC thereafter. This assessment is supported by process-based atmosphere-ocean modeling in combination with marine sediment data performed by Menviel and Joos (2012). They implemented the $\delta^{13}C$-based atmosphere-land flux, together with observation-based reconstruction of shallow water carbonate deposition (Vecsei and Berger, 2004) in the Bern3D dynamic ocean-sediment model. They demonstrate that simulated atmospheric CO_2 and $\delta^{13}CO_2$, as well as the spatio-temporal evolution of $\delta^{13}C$ of dissolved organic carbon (DIC) and carbonate ion concentrations in the deep ocean are fully consistent with the Holocene ice and marine sediment records.

Schneider et al. (2013) presented a high-resolution CO_2 and $\delta^{13}CO_2$ record for the Eemian that revealed several important differences between the Holocene and the Eemian dynamics of $\delta^{13}CO_2$. As Lourantou et al. (2010) who published the $\delta^{13}CO_2$ record during the onset of the Eemian, Schneider et al. (2013) found that the Eemian $\delta^{13}CO_2$ was by 0.2–0.3‰ lower than during the Holocene (Fig. 1). They suggested that one possibility to explain the generally lower atmospheric $\delta^{13}CO_2$ during the Eemian could be that less carbon was stored in the terrestrial biosphere. Hypothetically, this difference could be explained by carbon storage changes in permafrost, although there is no process-based model simulation yet which would support such a difference. Another possibility to explain this $\delta^{13}CO_2$ difference is a drift in the total ^{13}C inventory on 100 ka timescales due to imbalances in the input of ^{13}C by weathering, volcanic outgassing and the loss of ^{13}C by burial of organic carbon and calcium carbonate (Roth et al., 2014; Schneider et al., 2013; Tschumi et al., 2011). Secondly, they found that $\delta^{13}CO_2$ was not stable but experienced a rise and fall by 0.2‰ during the period of 122 to 116 ka. Schneider et al. (2013) argued that this fluctuation is partly explained by warmer SSTs at that time, thereby changing the fractionation during air/sea gas exchange, resulting in higher atmospheric ^{13}C values. Presumably, the difference between Holocene and Eemian in the CO_2 and $\delta^{13}CO_2$ dynamics could be explained by a difference in the forcings during these periods (orbital forcing, landuse forcing in the Holocene) and the memory effects associated with biogeochemical changes preceding the interglacials.

2.2. Overview of mechanisms governing interglacial CO_2 dynamics

The most recent interglacial period, the Holocene, is much better covered by the observational data than the earlier interglacial periods. For this reason, a majority of process-based modeling studies on interglacial carbon cycle encompass the Holocene (Brovkin et al., 2002, 2008; Foley, 1994; Joos et al., 2004; Kaplan et al., 2002; Kleinen et al., 2010; Menviel and Joos, 2012; Olofsson and Hickler, 2008; Ridgwell et al., 2003; Roth and Joos, 2012; Schurgers et al., 2006; Spahni et al., 2013; Stocker et al., 2011; Strassmann et al., 2008). Due to this wealth of previous research, our overview also strongly focuses on the Holocene. Most of the Holocene mechanisms, except for forcings linked to anthropogenic activity, are natural processes that should be active during all other interglacial periods as well. The confidence in the significance of these mechanisms during interglacials is quite different. Some of these processes are quantified in experiments using several models, and are clearly supported by geological evidence, while some mechanisms are hypothetical with currently insufficient understanding or poor quantitative support. We categorize well-understood mechanisms into terrestrial and marine processes, and then provide an overview of where large gaps in knowledge still remain.

2.2.1. Terrestrial mechanisms

2.2.1.1. Natural vegetation dynamics due to climate change and CO_2 fertilization. While the $\delta^{13}C$ of benthic foraminifera and the ^{18}O of atmospheric oxygen could be used as indirect proxies to constrain carbon transfer between the terrestrial biosphere and the ocean during glacial cycles (Ciais et al., 2012), no direct proxy exists for the past amount of carbon stored in terrestrial ecosystems. However, pollen-based reconstructions of terrestrial vegetation cover reveal changes in plant composition over the Holocene with up to decadal scale precision. During the Holocene climatic optimum, approximately 6000 years ago, the treeline in the high northern latitudes shifted northwards by several hundred kilometers in Asia and North America, and vegetation cover strongly increased in the northern subtropics from North Africa to the deserts in China (Prentice et al., 2000; Williams, 2003). The desertification of North Africa between 6 and 3 ka BP and the retreat of boreal forests from the Arctic coasts during the last 6000 years should have been accompanied by a substantial decrease in vegetation and soil carbon storage. Modeling studies by Foley (1994), Brovkin et al. (2002), and Schurgers et al. (2006) suggested that, indeed, carbon emissions of the order of several dozens to a hundred GtC could have been released to the atmosphere in the last 7000 years. However, Kaplan et al. (2002) and Joos et al. (2004) found that land acted as a carbon sink during this period. The difference between these modeling studies is explained by different climate forcings used by the ecosystem models and different model sensitivities to changes in climate and atmospheric CO_2. All models included a CO_2 fertilization mechanism, which leads to an increase in terrestrial carbon storage with growing CO_2 (e.g. Cramer et al. (2001)).

The physiological mechanisms and effects of increasing atmospheric CO_2, i.e. an increase of net photosynthesis and water-use efficiency, are well understood at the leaf level and considered in current models (Ainsworth and Rogers, 2007; De Kauwe et al., 2014). However, various mechanisms, such as nutrient constraints, lead to a sink limitation of photosynthesis and may attenuate this response at the plant and ecosystem scale (e.g.,Reich et al., 2014). Whether or not an attenuation of the leaf-level effect strongly occurs depends on the magnitude and time-scale of the CO_2 perturbation, for instance at centennial time-scales, minor changes in the ecosystem nitrogen budget may alleviate nitrogen constraints on CO_2 fertilization (Walker et al., 2015). Notwithstanding strong effects of nutrient constraints on plant production (Zaehle, 2013), there is limited understanding on how nutrient constraints would affect the terrestrial carbon balance at millenial time-scales.

The amplitude of the carbon storage increase depends on the

CO_2 sensitivity of the particular vegetation model and on the amplitude of the CO_2 increase in the model simulation (CO_2 could be prescribed or interactively simulated by the model). Moreover, many ecosystems are not only limited by CO_2, but by nutrient availability. All of these early modeling studies focused on changes in carbon storage in biomass and mineral soils, while neglecting changes in land carbon due to anthropogenic landuse and changes in organic soils including peatlands and frozen soils. Their main conclusion is that natural vegetation and soil dynamics responding to physical climate changes lead to a CO_2 source over the past 7 ka, while CO_2 fertilization leads to a land carbon sink, thus preventing land from being a net CO_2 source over this period. Eemian simulations with an interactive carbon cycle were performed by Schurgers et al. (2006). In their experiments, CO_2 concentrations increased by about 15 ppm between 128 and 115 ka due to a land source of about 300 GtC in response to a global cooling and the southward retreat of boreal forests.

2.2.1.2. Anthropogenic land use and land cover change. After publication of the Holocene CO_2 record by Indermühle et al. (1999), another hypothesis regarding the atmospheric CO_2 increase in the Holocene received prominent attention. Ruddiman (2003) argued that the increase in CO_2 during the last 8000 years of the Holocene is unique if one compares it with CO_2 dynamics in the previous interglacials. He suggested that the anomalous CO_2 growth was caused by anthropogenic land use beginning as early as 8000 years ago. The early human imprint on the atmospheric composition would also be found in atmospheric methane resulting from agricultural activities (rice cultivation, ruminants, wood burning). While there is no doubt that humans started to clear the land for early agriculture, the timing of the CO_2 increase, with by far the most dominant rise occurring from 7 to 5 ka BP, does not fit population dynamics and the evolution of agricultural expansion. Numerous modeling studies (Brovkin et al., 2004; Joos et al., 2004; Olofsson and Hickler, 2008; Pongratz et al., 2009; Stocker et al., 2011; Strassmann et al., 2008) based on population and land use scenarios such as HYDE (Goldewijk et al., 2011) found that an effect of land use emissions on atmospheric CO_2 before 1850 is not larger than a few ppm. Only one modeling study by Kaplan et al. (2011) based on large area-per-capita usage by early societies and large soil carbon depletion after land conversion suggested that cumulative carbon emissions resulting from anthropogenic land clearance before 3 ka BP caused an atmospheric CO_2 increase of 7 ppm. Ruddiman (2013) used the Neolithic modeling study by Wirtz and Lemmen (2003) to support the hypothesis of early Holocene land use, but modeling of human population dynamics remains to be highly uncertain. In addition, the Holocene trend of atmospheric methane measured in ice cores – which is also an important byproduct of fire activity (mostly in the smoldering phase) – combined with the rather constant $\delta^{13}CH_4$ signal over the last 4000 years (Sowers, 2010) also does not favor a scenario with a substantial change in fire CH_4 emissions caused by human activities. Such changes related to humans and land use are apparent only during the last 2000 years (Sapart et al., 2012). The most important data constraint on the early anthropogenic hypothesis comes from the carbon isotopes in atmospheric CO_2, as land use-related carbon emissions should have caused a negative $\delta^{13}CO_2$ signal, which is significantly larger than the signal suggested by analysis of the $\delta^{13}CO_2$ record (Elsig et al., 2009; Schmitt et al., 2012). It is more plausible to assume that land use played some role in the CO_2 increase during the last millennium (e.g., Bauska et al., 2015), but cannot explain the whole CO_2 growth from 7 to 1 ka. A large spread in the amplitude of landuse emissions is one of the major sources of uncertainties in simulations of CO_2 dynamics during the Holocene. The high-end emission scenarios such as the one by Kaplan et al. (2011) require large areas of conversion from forests to open landscapes, which cannot be left unnoticed in the pollen records. The most reliable approach to constrain the landuse emissions is to use pollen records to reconstruct changes in tree cover (Williams, 2003) and land use (Fyfe et al., 2015; Gaillard et al., 2010) during the Holocene. Until such a large–scale, time-resolved synthesis is available, carbon cycle modelers are forced to test different land-use scenarios to address uncertainties in population-based estimates in historical land use (Stocker et al., 2011).

2.2.1.3. Fire activity. Fires are a major component of vegetation and land use change, where fire activity includes both anthropogenic and natural aspects. Humans have conducted large-scale land clearance using fires for millennia with the goal of opening land for agriculture, or using fire as a hunting tool (Bowman et al., 2009; Power et al., 2013). The timing and spatial extent of such human-induced fire activity varies by region. Temperate zones in Southern Europe and East Asia were among the first areas to be subject to anthropogenic deforestation (Kaplan et al., 2009; Yang et al., 2013), with major burning beginning in the mid-Holocene, where native forests never recovered but remained primarily agricultural or urban land. Climate is another main driver of fire activity. With increased temperature, fire activity generally escalates, affecting carbon fluxes (Bowman et al., 2009; Flannigan et al., 2009). Drier conditions also result in greater fire activity, but only up to the point in which the arid conditions still provide sufficient amount of biomass to burn (Marlon et al., 2012). Charcoal syntheses from primarily temperate regions demonstrate that over the past 21,000 years (Power et al., 2008) and over the Holocene (Marlon et al., 2013) climate has been the major driver of fire activity. Modeling studies (Bruecher et al., 2014; Kloster et al., 2015) also suggest that the fire trend in the Holocene is mainly driven by trends in aridity and changes in fuel storage due to productivity changes. Antarctic ice core records reveal that fire activity closely correlates with climate over the past 2000 years until industrial period (Ferretti et al., 2005; Wang et al., 2010). Multiple proxies in Greenland ice cores provide a more comprehensive picture. Climate has a main influence on boreal fire activity over the past 2000 years, with peak fire activity coincident with major Central Asian droughts in the 1600s AD (Zennaro et al., 2014), while the biomass burning maximum in Europe about 2500 years ago may be due to anthropogenic land clearance (Zennaro et al., 2015).

2.2.1.4. Peat accumulation. During the last termination and after the onset of the Holocene about 11,700 years ago, large areas with relatively flat terrain in northern Eurasia and North America became moist and warm during the summer, enabling the development of peatlands. ^{14}C-based reconstructions of peat basal ages in the boreal regions revealed a peak in the initiation of peatlands during 11 to 9 ka, and boreal peatland formation continued throughout the entire Holocene (Loisel et al., 2014; MacDonald et al., 2006; Yu et al., 2010b). Currently existing northern peatlands have accumulated 230 to 550 GtC over the past 15 ka ((Yu, 2012) and references therein), with the most recent estimate of 436 GtC (Loisel et al., 2014), while tropical and southern hemisphere peatlands accumulated about 50 and 15 GtC, respectively (Yu et al., 2010b). However, part of the newly accumulated peat should be compensated by widespread drying of existing peatlands or peatlands submerged under sea water on ocean shelves (Dommain et al., 2014) from the last glacial and the time immediately thereafter. While the accumulation on presently existing peatlands is supported by modeling results (Kleinen et al., 2015, 2012; Spahni et al., 2013), there is yet a lack of studies that address the temporal balance between carbon loss from disappearing peatlands and carbon gain on establishing peatlands.

Loisel et al. (2014) find the highest carbon accumulation rates in boreal peatlands during 11 to 7 ka BP, and an overall slowdown of peat accumulation rate during the mid- and late Holocene, with minimum values during 3 to 1.5 ka BP. While quantifying a net effect of peatlands on atmospheric CO_2 is challenging, we can hypothesize that the carbon uptake by boreal peatlands likely contributed to the early Holocene CO_2 decrease. This uptake is also an important driver for the land carbon uptake of ~290 GtC between 11 and 5 ka BP inferred from the deconvolution of the CO_2 and $\delta^{13}CO_2$ ice core data (Elsig et al., 2009). The continued accumulation of boreal peat after 5 ka BP should have led to a decrease in atmospheric CO_2, and a corresponding increase in atmospheric $\delta^{13}CO_2$ in the Holocene, which is the opposite of the observed small negative trend (Fig. 1a). Consequently, the peat sink over the past 5 ka has to be compensated by another source of isotopically light CO_2. A carbon uptake by peat buildup during the Holocene cannot bring the atmospheric ice core observations and the early anthropogenic hypothesis by Ruddiman (2003, 2013) in agreement. A peat buildup simultaneous to landuse-induced carbon release could stabilize the $\delta^{13}CO_2$ values over the last 7000 years, but then landuse cannot cause the atmospheric CO_2 increase over the same time period. In addition, the timing and evolution of peat build up does not agree with CO_2 emissions from landuse, as peat build-up is very linear and steady over the entire Holocene (Kleinen et al., 2012; Loisel et al., 2014; Spahni et al., 2013), while an increase in landuse emissions over the past 7 ka cannot be linear due to non-linear population growth.

All considered terrestrial processes affect carbon storage on land and have negative $\delta^{13}C$ signatures (ca. −25‰ for C_3-photosynthesis plants). Uptake or release of terrestrial carbon therefore leads to an increase or decrease in atmospheric $\delta^{13}CO_2$.

2.2.2. Marine mechanisms

2.2.2.1. Changes in SSTs. Increasing temperature of surface waters leads to CO_2 outgassing and consequently to an increase in atmospheric CO_2. In equilibrium, the dependency of atmospheric CO_2 on SST due to CO_2 solubility (Henry's law) leads to an atmospheric CO_2 sensitivity to uniform temperature change of about 9–10 ppm/°C (Archer et al., 2004). Indermühle et al. (1999) considered proxy data on increasing tropical SSTs as a global signal and proposed an increase in SSTs as an important mechanism of CO_2 growth during the Holocene. However, tropical warming in the course of the Holocene was accompanied by a SST decrease in the North Atlantic (Kim et al., 2004; Marchal et al., 2002). Because Atlantic deep waters are formed in the northern high latitudes, the surface cooling in this region should have a disproportionally stronger effect on the carbon transfer to the ocean in comparison with the effect of SST changes in low latitudes. Modeling studies by Brovkin et al. (2002) and Menviel and Joos (2012) found almost no CO_2 effect in response to the small increase in global SSTs during the last 7 ka. Direct forcing of biogeochemistry models with SSTs reconstructed by Kim et al. (2004) led to a small decrease in atmospheric CO_2 (Brovkin et al., 2008). In line with these studies, Goodwin et al. (2011) estimated the effect of simulated SSTs from 8 ka to the pre-industrial as a drop of CO_2 of only 0.1–1.1 ppm. In summary, the effect of changes in SSTs on atmospheric CO_2 during the Holocene is likely to be small, and on the order of a few ppm (Schmitt et al., 2012).

2.2.2.2. Carbonate compensation due to deglaciation and terrestrial biosphere growth. The carbonate compensation mechanism (Broecker et al., 1999) is a response of the ocean carbonate chemistry to changes in boundary conditions, such as atmospheric CO_2 concentrations or oceanic circulation. Large-scale reorganization of ocean circulation and the carbon cycle during the last deglaciation likely led to the release of large amounts of CO_2 from the ocean. After CO_2 release, bottom waters should become less acidic and lead to a preserved spike in $CaCO_3$ in marine sediments, which, indeed, is prominent in marine cores during deglaciations (Broecker et al., 1999; Farrell and Prell, 1989). Carbonate compensation due to this re-organization - a process of restoring a balance between terrestrial weathering and carbonate sedimentation in the ocean - has a long timescale of 5–7 thousand years. During this period, the alkalinity removal due to carbonate sedimentation in the deep ocean is higher than the alkalinity input due to weathering. This imbalance between input and removal leads to a reduction in total ocean alkalinity and an additional release of CO_2 to the atmosphere since less alkane water contains less DIC. Because of the millennial time scale of carbonate compensation, the carbonate system was in disequilibrium at the beginning of the Holocene, and this should also have a small elevating effect on atmospheric CO_2 during the Holocene. This disequilibrium effect could be quantified in a transient simulation using a climate-carbon cycle model during deglaciation (Brovkin et al., 2012; Menviel and Joos, 2012; Menviel et al., 2012), but it is also superimposed by the following two processes that affect marine carbonate chemistry during interglacials.

Marine carbonate chemistry responds to the uptake of several hundred Gt of carbon by terrestrial ecosystems during the early Holocene and the previous glacial termination (~18–11 ka BP). The land carbon uptake led to a small decrease of CO_2 by ca. 5 ppm from 11 to 8 thousand years ago (Fig. 1). In response to this carbon uptake and atmospheric CO_2 drop, oceans should become less acidic and carbonate sedimentation should increase, leading to reduced alkalinity and CO_2 release to the atmosphere as discussed in the previous paragraph (Broecker et al., 1999, 2001). For the period from 7 to 0 ka BP, this effect is estimated as about 5 ppm to compensate for early Holocene land uptake and between 0 and 5 ppm in response to land uptake over the glacial termination (before 11 ka BP) (Joos et al., 2004; Menviel and Joos, 2012).

2.2.2.3. Enhanced shallow-water carbonate sedimentation. Increased shallow-water carbonate sedimentation could have been a dominant contributor to the CO_2 growth during the Holocene. During deglaciations, when tropical shelves are flooded, corals and other calcifying organisms start to accumulate large amounts of $CaCO_3$ in tropical and subtropical shallow waters. Estimated excessive global $CaCO_3$ accumulation rates in shallow waters vary between 2.9 (0.03) (Vecsei and Berger, 2004) and 12 (0.14) Tmol/yr (GtC/yr) at present (Milliman, 1993; Opdyke and Walker, 1992). Because total $CaCO_3$ sedimentation in equilibrium is limited by the weathering flux, more burial on shelves leads to less burial in the deep sea. This redistribution of carbonate sedimentation leads to a reduction in total alkalinity on global scale, which leads to a release of CO_2 to the atmosphere (see previous section). Brovkin et al. (2002), Ridgwell et al. (2003), Kleinen et al. (2010), and Menviel and Joos (2012) found this mechanism to be a strong contributor to the atmospheric CO_2 growth during the Holocene.

Marine processes discussed in Section 2.2 do not have a significant impact on atmospheric $\delta^{13}CO_2$. Changes in SSTs influence the isotopic fractionation of CO_2 at the ocean surface (Marchal et al., 1998), however, the effect is small because of the geographical pattern of SST changes (Brovkin et al., 2002). Fluxes of carbonate and weathering have a ^{13}C isotopic signature close to zero and, therefore, have almost no influence on the oceanic $\delta^{13}C$ and atmospheric $\delta^{13}CO_2$.

2.2.3. Processes with large gaps in knowledge

2.2.3.1. Permafrost carbon changes. Recently, the attention of carbon cycle modelers turned towards organic matter stored in permafrost soils. Permafrost and peatlands are not mutually

exclusive terms as parts of peatland areas are also permafrost areas. Large-scale syntheses by Tarnocai et al. (2009) and Hugelius et al. (2014) revealed that the current storage of carbon in frozen soils, including deltaic alluvium and Yedoma sediments, is on the order of 1300 GtC. This carbon was mainly accumulated during the glacial period in regions free of ice sheets. For instance Ciais et al. (2012) estimated that 2300 GtC were stored as an inert carbon pool during the LGM. In the ice-rich land complexes in the Arctic, carbon storage reaches densities of several hundred $kgCm^{-2}$. During deglaciation, when the total permafrost area nearly halved (Saito et al., 2013), part of the permafrost carbon would have decomposed quickly and affect both atmospheric CO_2 and $\delta^{13}CO_2$ (see Section 2.1). Nonetheless, processes of thermal erosion and thermokarst formation are continuing in the Holocene, as well as the development of new permafrost. The balance of these processes on large scales is difficult to estimate, but modeling studies suggest that the accumulation of carbon in newly formed permafrost areas prevails over decay in the late Holocene (Crichton et al., 2014), although processes of thermokarst formation and thermal erosion are not yet included in these models. Walter Anthony et al. (2014) used observational evidence to suggest that thermokarst lakes turned from carbon sources to sinks during the Holocene. The buildup of permafrost carbon is unlikely to continue in the future due to anthropogenic climate change.

2.2.3.2. Enhanced volcanic outgassing. On geological time scales, the burial of organic carbon and $CaCO_3$ in marine sediments is compensated by volcanic CO_2 outgassing. Present-day estimates of subaerial emissions are in the range of 0.02–0.15 GtC/yr (Burton et al., 2013; Gerlach, 2011). Roth and Joos (2012) concluded that enhanced volcanic CO_2 emissions in response to disintegration of ice sheets proposed by Huybers and Langmuir (2009) possibly contributes to the CO_2 rise during deglaciation, but not during the late Holocene. On considered timescales, volcanic CO_2 emissions have almost no influence on atmospheric $\delta^{13}CO_2$ since their ^{13}C isotopic signature is close to zero.

2.2.3.3. Reduction in storages of marine CH_4 hydrates. One of the least known processes is the response of methane hydrates in marine sediments on continental slopes and on the Arctic shelves. The sensitivity of marine hydrate storage to an increase in the bottom temperature depends on the value of the critical bubble fraction enabling gas escape from the sediment column. This release is estimated to be about 30–500 GtC in response to 3 °C warming (Archer et al., 2009). Most of this methane will be oxidized in the water column and will only reach the atmosphere as carbon dioxide (Reeburgh, 2007). Because propagation of the heat signal through the sediments has a time scale of several thousand years, the warming of shallow and intermediate waters during the deglaciation could have led to an additional source of isotopically light carbon (ca. −50 to −60‰) which contributed to the decrease in atmospheric $\delta^{13}CO_2$ during the course of the Holocene. The scale of this effect is difficult to estimate with current methane hydrate models. A destabilization of metastable CH_4 hydrates in sub-sea permafrost in response to the shelf flooding might be responsible for present-day elevated CH_4 concentrations in the Laptev Sea region (Shakhova et al., 2014). Hydrogen isotopic measurements on atmospheric methane in ice cores did not support clathrate destabilization during rapid warming events in Marine Isotope Stage (MIS) 3 (Bock et al., 2010) or during the last deglaciation (Sowers, 2006). These ice-core reconstructions do not contradict a possible impact of CH_4 hydrates on atmospheric CO_2, as most of the methane emitted at the seabed is oxidized in the water column (Reeburgh, 2007).

2.2.3.4. Reduction in the ocean soft tissue pump. Reduction in the ocean soft tissue pump corresponds by definition (Volk and Hoffert, 1985) to a less efficient utilization of surface nutrients and a corresponding decrease in the export of biological material out of the surface layer. These changes lead to higher pCO_2 in the surface ocean, and as a result, to higher atmospheric CO_2 and lower atmospheric $\delta^{13}CO_2$. Although there is no evidence of large-scale changes in the ocean soft issue pump in the Holocene, Goodwin et al. (2011) used marine $\delta^{13}C_{DIC}$ data to demonstrate that the role of this mechanism in the CO_2 increase during the last 8 ka could be significant.

2.3. Proxy constraints on interglacial carbon cycling

Beyond the high quality atmospheric measurements from Antarctic ice cores (Fig. 1), there are other, less direct proxies, which help to understand the mechanisms behind interglacial CO_2 changes. Terrestrial pollen records represent valuable geological archives describing changes in the distribution of vegetation cover during glacial-interglacial transitions and interglacials. These records can be used for model-data comparisons in terms of dynamics of forests and bare ground during interglacials (Kleinen et al., 2011), while their interpretation in terms of changes of carbon storages is more qualitative than quantitative. For the Holocene, these records show that the northern tree line was in a more northerly position at 6 ka BP both in Eurasia and North America (Prentice et al., 2000; Williams, 2003). Similarly, changes are visible for the forest-steppe boundary in Eurasia (Kleinen et al., 2011) and the Sahel-Sahara boundary, where the Sahel area expanded northwards at 6 ka BP (Prentice et al., 2000; Shanahan et al., 2015). For previous interglacials, terrestrial pollen archives are less informative since areas in the high northern latitudes, where changes took place during the Holocene, were severely affected by glaciation, eradicating any evidence that might have been used to reconstruct vegetation for previous interglacials. Nonetheless, evidence from ice–free areas like Lake El'gygytgyn in eastern Siberia indicates tree cover changes similar to the Holocene, where a northerly movement of trees in the early interglacial followed a change to tundra conditions (Tarasov et al., 2013).

Lake sediment charcoal records provide evidence of past fire activity and associated CO_2 emissions. Charcoal primarily comes from organic matter (wood, grass) exposed to high temperatures. These temperatures drive off volatile elements and leave a carbon residue that can be transported tens of kilometres from the source and deposited in lake, marine and peat sediments. Physical counting of charcoal particles and their chemical analysis provide detailed records of fire activity in vast areas. The Global Charcoal Database (GCD) is a global syntheses effort (Power et al., 2008) that enables examining broad-scale patterns in paleo-fire activity since LGM (21.000 BP). Several Holocene data studies focus on the climatic controls of fire (e.g., Marlon et al., 2013) or on model-data comparisons (Bruecher et al., 2014) to understand natural wild fire in the past. Global fire activity increased over the Holocene, but the driving factors differ among regions and may offset each other (Kloster et al., 2015). Charcoal data sets are reported in Z-scores which are very useful for reconstructing temporal and spatial trends in fire activity, but not applicable for quantitative reconstructions of burned area, carbon emissions by fire, or the original burned fuel. Due to the harmonization process to obtain a global trend (Power et al., 2008), an increase in reported Z-scores could be related to a decrease in burned area. Therefore, comparisons on regional or local scales are more meaningful.

Deep-sea carbonate sediments provide another useful archive for evaluating mechanisms of interglacial CO_2 changes. Over the course of the Holocene, the data show a decrease in carbonate ion

concentrations in the deep Pacific (Yu et al., 2010a) where the dissolution of the deep sea carbonate sediments in the Pacific continues through the Holocene (Anderson et al., 2008). The dissolution of deep sea sediments could be a response to the redistribution of carbonate sedimentation from the deep sea to shallow seas, to the CO_2 release from the terrestrial biosphere, or the re-partitioning of sinks within the ocean in response to large-scale changes in ocean circulation (Chikamoto et al., 2008). Therefore, the dissolution cannot verify whether the source of carbon to the atmosphere has marine or terrestrial origin. Goodwin et al. (2011) used a theoretical model framework to demonstrate that changes in SSTs do not impose a strong constraint on the sources of carbon for the atmospheric CO_2 increase during the Holocene. They argued that the inclusion of marine $^{13}C_{DIC}$ data, in addition to the combination of carbonate ion concentration and atmospheric $\delta^{13}CO_2$, reduces the uncertainty in the reconstruction of CO_2 sources during the Holocene.

3. Methods

3.1. Models

Our overall approach is to utilize three established Earth system models that differ in two key characteristics – the representation of ocean circulation (and hence marine carbon cycling) and the representation of terrestrial carbon storage dynamics and vegetation, hence giving us some measure of the model uncertainty. We emphasize that we do not include all major driving factors in our simulations as well as legacy fluxes from changes prior to the starting point of our simulations for simplicity and comparability among models. Thus, we cannot expect that model results will agree with proxy data. The model descriptions are summarized first, followed by our experimental design.

3.1.1. Bern-3D model

The Bern3D-LPJ climate–carbon-cycle model (hereafter Bern3D) is an EMIC that includes an energy and moisture balance atmosphere and sea ice model (Ritz et al., 2011), a 3-D dynamic ocean (Muller et al., 2006), a marine biogeochemical cycle with prognostic formulations for marine export production (Parekh et al., 2008; Tschumi et al., 2008), an ocean sediment model to simulate redissolution and burial flux for opal, calcium carbonate, and organic matter (Tschumi et al., 2011), and the LPJ dynamic global vegetation model (Joos et al., 2004; Sitch et al., 2003; Stocker et al., 2011). Weathering and volcanic fluxes are kept constant. The model is used with a resolution of 36 × 36 grid cells in the horizontal domain and 32 layers within the ocean. The LPJ model was used here on a spatial resolution of 3.75° (longitude) by 2.5° (latitude) in a simplified model setup (Stocker et al., 2011) without recently developed modules for wetlands and peatland area (Stocker et al., 2014) and peat carbon dynamics (Spahni et al., 2013) as we use prescribed peat accumulation scenarios. An earlier version of LPJ that does not include nitrogen dynamics leads to realistic estimates of growth responses to CO_2 fertilization (Hickler et al., 2008). The climate model maps monthly temperature and precipitation anomalies relative to a preindustrial climate. These anomalies are passed to LPJ once per year and applied to a modern Climatic Research Unit (CRU) climatology (New et al., 2000) in the LPJ model. Carbon isotopes are simulated interactively in all model components with fractionation factors depending on environmental conditions.

3.1.2. CLIMBA

CLIMBA (Bruecher et al., 2014) consists of the EMIC CLIMBER-2 (CLIMate and BiosphERe) (Ganopolski et al., 2001; Petoukhov et al., 2000) and JSBACH (Brovkin et al., 2009; Raddatz et al., 2007; Reick et al., 2013; Schneck et al., 2013), which is the land component of MPI-ESM (Giorgetta et al., 2013). While CLIMBER-2 simulates the atmosphere and land processes at roughly 51° (longitude) by 10° (latitude), the JSBACH model runs on higher spatial resolution (3.75° longitude by 3.75° latitude) including a daily cycle to better resolve heterogeneous land processes. Similar to the Bern3D model, JSBACH is driven by climate anomalies from CLIMBER-2 including temperature, precipitation, radiation balance, and atmospheric CO_2 concentration and feeds back changes in the land carbon to CLIMBER-2 as a flux to the atmosphere. CLIMBER-2 includes a conventional oceanic biogeochemistry model (Brovkin et al., 2002) and a deep-sea carbonate sediment model (Archer, 1996), as well as a module for long-term processes of weathering and volcanic outgassing. Weathering fluxes scale to runoff from the land surface grid cells, with separate carbonate and silicate lithological classes (Brovkin et al., 2012). Consequently, weathering fluxes are different for the Eemian and Holocene conditions due to differences in runoff (Brovkin et al., 2012). Volcanic emissions of CO_2 are assumed to be constant at 0.07 GtC/yr (Gerlach, 2011).

3.1.3. GENIE

The version of GENIE (Grid Enabled Integrated Earth System model) EMIC used here is a coupled ocean carbon cycle - climate model. The climate component is based on the fast climate model of Edwards and Marsh (2005), which includes a reduced physics 3-D ocean circulation model coupled to a 2-D energy-moisture balance model of the atmosphere and a thermodynamic sea-ice model. The ocean carbon cycle model includes a representation of the preservation and burial of calcium carbonate in deep sea sediments (Ridgwell and Hargreaves, 2007; Ridgwell et al., 2007). In addition, a weathering module calculates the solute supply to the coastal ocean resulting from the weathering on land of exposed rock surfaces and soil minerals (Colbourn et al., 2013). The land carbon component is not included.

3.2. Simulations setup

To investigate the effect of several forcings on atmospheric CO_2, we first ran a set of simulations for both Holocene and Eemian periods (Table 1). The simulation Holo_All was used with a standard setup of forcings to simulate Holocene climate and carbon dynamics from 8 to 0.5 ka. The orbital forcing is after Berger and Loutre (1991); the shallow water sedimentation is 4.88 Tmol $CaCO_3$/yr from 8 to 6 ka BP and 3.35 Tmol $CaCO_3$/yr from 6 to 0 ka BP in accordance with Vecsei and Berger (2004); the landuse

Table 1
Simulation setup.

Simulation	Orbital forcing	$CaCO_3$ accumulation	Landuse	Peat
Holocene (8 to 0.5 ka BP)				
Holo_All	Yes	V&B[a]	HYDE[b]	No
Holo_Peat	Yes	V&B	HYDE	Yes
Holo_12T	Yes	O[c]	HYDE	No
Holo_Kc	Yes	V&B	Kc[d]	No
Holo_noO	No	V&B	HYDE	No
Eemian (126 to 115 ka BP)				
Eem_All	Yes	V&B	No	No
Eem_noO	No	V&B	No	No
Eem_Peat	Yes	V&B	No	Yes
Eem_12T	Yes	O	No	No

[a] (Vecsei and Berger, 2004).
[b] (Goldewijk et al., 2011).
[c] (Opdyke and Walker, 1992).
[d] Emissions from the Bern3D model driven by Kaplan et al. (2011) landuse scenario.

emissions follow the HYDE dataset (Goldewijk et al., 2011; Stocker et al., 2011). The simulations were repeated using the same forcings as in Holo_All with the following changes: without orbital forcing (Holo_noO); with peat accumulation of 25 GtC/ka (Holo_P); with Kaplan et al. (2011) areal landuse scenario but using the Bern3D model to simulate the landuse emissions (Holo_Kc); with carbonate accumulation scenario by Opdyke and Walker (1992) of 12 Tmol $CaCO_3$/yr from 8 to 0 ka BP (Holo_12T). Secondly, the same simulations, but without landuse scenarios, were conducted for the Eemian period from 126 to 115 ka (Eem_All, Eem_noO, Eem_P, Eem_12T).

The initial spinup of the carbon cycle models was performed with the following boundary conditions: atmospheric CO_2 concentration in the initial setup was equal to 260 and 276 ppm and atmospheric $\delta^{13}CO_2$ to −6.4 and −6.7‰ for 8 ka and 126 ka BP, respectively. The ^{13}C discrimination of accumulated peat and landuse emissions was taken as 18‰ assuming the C_3-type photosynthesis. In terms of $\delta^{13}C$, peat carbon is depleted due to fractionation processes involved in *Sphagnum* moss production (Loisel et al., 2009). All models calculated atmospheric CO_2 concentration interactively: simulated changes in atmospheric CO_2 led to changes in marine and terrestrial carbon uptake (including CO_2 fertilization), as well as climatic changes. Atmospheric $\delta^{13}CO_2$ was calculated interactively by Bern3D and GENIE. The JSBACH model in CLIMBA does not include an interactive ^{13}C cycle, therefore the atmospheric $\delta^{13}CO_2$ was calculated diagnostically by using simulated JSBACH fluxes and assuming the average ^{13}C discrimination of land carbon to be 15‰. The carbonate accumulation in the deep sea followed each model approach to simulate equilibrium carbonate sedimentation. For example, CLIMBA simulated carbonate sedimentation in the pre-Holocene equilibrium simulation by redistributing the carbonate from shallow water to the deep ocean assuming that coral sedimentation in pre-Holocene conditions was 2 Tmol/yr (Kleypas, 1997) as done by Kleinen et al. (2015). At the beginning of interglacial simulations, an additional carbonate accumulation - in accordance with either Vecsei and Berger (2004) or 12 Tmol/yr scenarios - was added to the sedimentation level of 2 Tmol/yr. The Bern3D and CLIMBA models have an interactive land carbon cycle, while GENIE includes only the marine carbon cycle. A land-sea mask fixed to pre-industrial conditions was not changed during simulations. Changes in forcings of N_2O and CH_4 were not accounted for.

We address the role of terrestrial carbon mechanisms (landuse, peat), and shallow-water $CaCO_3$ sedimentation by changing the scale of these forcings or by switching them off in the model runs. Natural vegetation dynamics, CO_2 fertilization, and wildfires were interactive in Bern3D and CLIMBA. SSTs changes were addressed using GENIE simulations. We did not consider the delayed responses of carbonate compensation to deglaciation and terrestrial carbon changes in the early Holocene as they require non-stationary initial conditions. The role of permafrost carbon, volcanic outgassing and methane hydrates remains poorly quantified up to now and therefore are not addressed in our simulations.

4. Model results and discussion

4.1. Changes in CO_2 and $\delta^{13}CO_2$

Comparison of simulated CO_2 dynamics in the Holo-All and the Eem-All experiments with ice core data is shown in Fig. 2a and b for the Holocene and Eemian, respectively. For the Holocene, all three models simulate CO_2 changes close to the data during the period of 8 to 6 ka BP, but afterwards simulate a smaller rate of CO_2 increase than in the data. By 0.5 ka BP, the Bern3D model is at the highest level of 274 ppm, while the CLIMBA and GENIE models simulate CO_2 concentration of ca. 270 ppm, explaining half of the 20 ppm changes reconstructed for the period from 8 to 0.5 ka BP. For the Eemian period, the simulated CO_2 concentration is close to the observed record from 126 to 121 ka BP for all models, but it departs afterwards with higher CO_2 levels than those shown in the reconstructed data. CO_2 simulated by the GENIE model slowly approaches stabilization level after 121 ka BP, while Bern3D and CLIMBA models simulate strong increases in CO_2 until 117 ka BP and levels off afterwards. This strong difference between models is due to absent terrestrial fluxes in the GENIE model, as the two other models simulate a strong decrease in terrestrial carbon storage after 122 ka BP that leads to an increase in atmospheric CO_2.

The $\delta^{13}CO_2$ simulated by the Bern3D and CLIMBA models mainly reflect changes in terrestrial carbon. During the Holocene, both models show a small increase by 0.05‰ at the beginning of the simulations and then an almost constant level of $\delta^{13}CO_2$ with a small offset between them due to a difference in the initial conditions (Fig. 2c). For the Eemian, the GENIE model simulates a small overall trend in atmospheric $\delta^{13}CO_2$, reflecting the absence of terrestrial biosphere changes in this model. No model, in combination with the imposed forcing and spin-up procedure, is able to explain the increase and drop in $\delta^{13}CO_2$ between 122 and 116 ka BP as seen in the reconstructed data. Direct interpretation of this upward excursion of 0.2‰ would require an increased land or marine biological uptake of several hundred GtC, which is opposite to the expected results of the current generation of terrestrial carbon cycle models. As noted above, our model spin-up and protocol by design do not consider all relevant mechanisms, e.g. peat and permafrost carbon dynamics, as interactive components. We also used equilibrium initial conditions, therefore neglecting longer-term imbalances in the carbon cycle and carbonate system during the preceding terminations. Therefore, we do not expect that the model simulations will fit observations.

4.2. Changes in biomass, mineral soil carbon, and tree cover

The effects of climatic and CO_2 forcings on terrestrial carbon storages in Bern3D and CLIMBA in the Holo-All and the Eem-All is shown in Figs. 3–7. The Bern3D model simulates a carbon storage that is 20 GtC higher at 8 ka BP than at 0.5 ka BP (Fig. 3a). Most of this carbon is accumulated in the northern high latitudes in response to temperature increases in these regions, in line with the orbital forcing changes. Because of lower CO_2 levels at 8 ka, the changes in storage in temperate latitudes are negative. CLIMBA does show small increases in terrestrial carbon storage in northern Siberia and Alaska, but overall the model has ca. 75 GtC less terrestrial carbon at 8 ka than at 0.5 ka (Fig. 3c). This difference is due to a weak effect of the climate anomalies (Fig. 5a) on carbon and due to a strong CO_2 fertilization effect in the model. For the Eemian, however, both models show more agreement in the changes in carbon storage on land (Fig. 3b, d). Both CLIMBA and Bern3D simulate 120–130 GtC more carbon at 126 ka than at 115 ka BP, with most of this carbon accumulated in the high northern latitudes in response to climate change.

The response of annual land air surface temperature to the Holocene forcing is slightly different between the models. There is a minor temperature increase by 0.2 °C in the Bern3D model (Fig. 4a), while the temperature in the CLIMBA model decreases by 0.2 °C (Fig. 5a) from 8 to 0.5 ka BP. This increase in the Bern3D model is a result of superimposed drivers of increasing CO_2 and cooling in the northern high latitudes due to orbital forcing changes. Reconstructions by Marcott et al. (2013) show a decrease by about 0.6–0.8 °C in global annual mean temperature from 8 to 0.5 ka, however, such a significant cooling trend is not supported by models (Lohmann et al., 2013). During the last interglacial, both

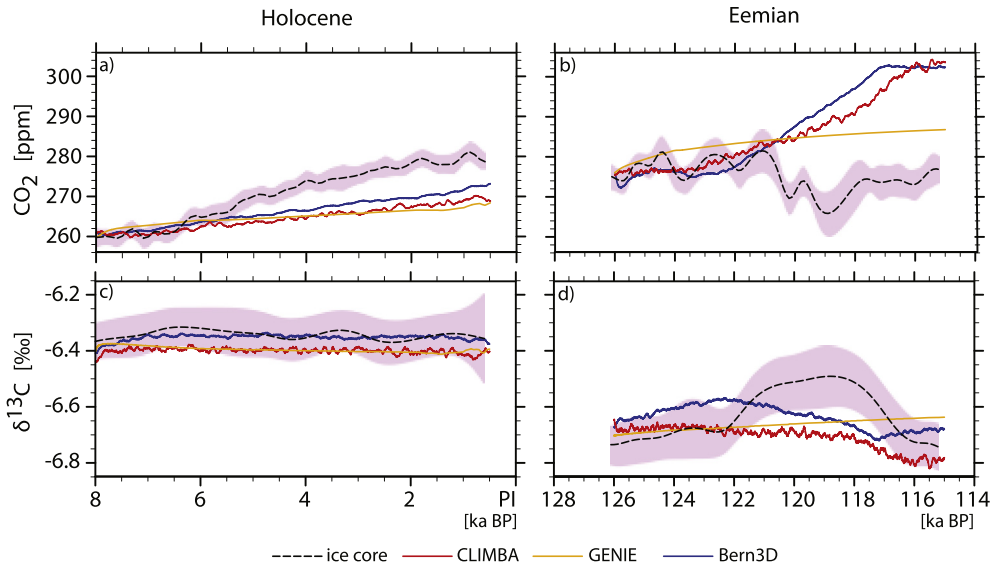


Fig. 2. Simulated dynamics of atmospheric CO_2 concentration, ppm (a, b) and $\delta^{13}CO_2$, ‰ (c, d) during the present (a, c) and the last (b, d) interglacial in Holo_All and Eem_All, respectively, against ice core data reported in Fig. 1.

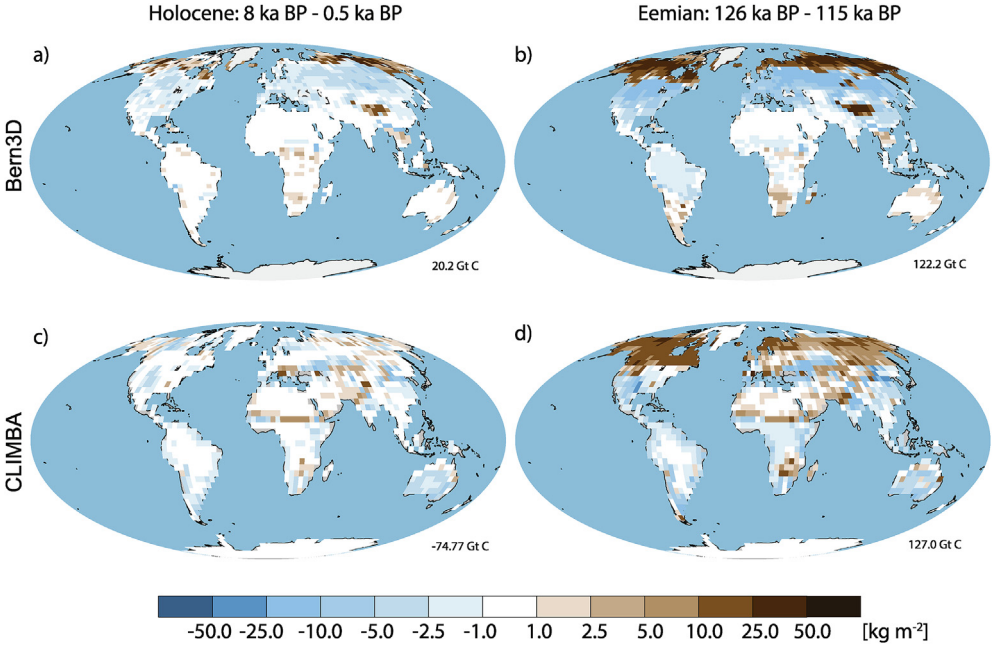


Fig. 3. Maps of changes in the total land carbon storage for the Holocene between 8 and 0.5 ka BP (a, c) and for the Eemian between 126 and 115 ka BP (b,d) in Holo_All and Eem_All, respectively. Bern3D model (a, b) and CLIMBA (c, d).

models reveal a decreasing trend in global temperature by ca. 1.5 °C (Figs. 4b and 5b), despite the modeled increase in the atmospheric CO_2 by almost 30 ppm. The latitudinal pattern of warming at 126 ka BP is very similar in both models. The warming is pronounced in both northern and southern hemispheres, and is especially strong for latitudes north of 30°N.

The temporal evolution of the terrestrial biomass response to changes in climate and CO_2 differs among the models. In the Bern3D model, the total biomass (green carbon) increases in the Holocene (Fig. 4c), while during the Eemian the biomass first increases and then subsequently decreases (Fig. 4d). In the CLIMBA model, total terrestrial biomass does not change much during both periods (Fig. 5c, d), as biomass decrease in the high latitudes is compensated by its increase in the tropical regions, in line with changes in the orbital forcing. Both models show similar latitudinal patterns in the soil carbon changes during both interglacials. The main increase in the mineral soil carbon at 8 and 126 ka BP occurs in the latitudes north of 60°N (Fig. 4e, f; Fig. 5e, f). Soil carbon storages decrease during the Holocene by 40 GtC in the Bern3D model (Fig. 4e), while increasing by 70 GtC in the CLIMBA model (Fig. 5e). In the Eemian, the maximum carbon storage in biomass and mineral soil carbon occurs at 122 ka BP in both models (Figs. 4f and 5f). Afterwards, both soil and biomass carbon storages quickly decrease in both the Bern3D and CLIMBA models. This contributes to the CO_2 growth during the period (Fig. 2b) and is reflected in a strong decreasing signal in atmospheric $\delta^{13}CO_2$ (Fig. 2d).

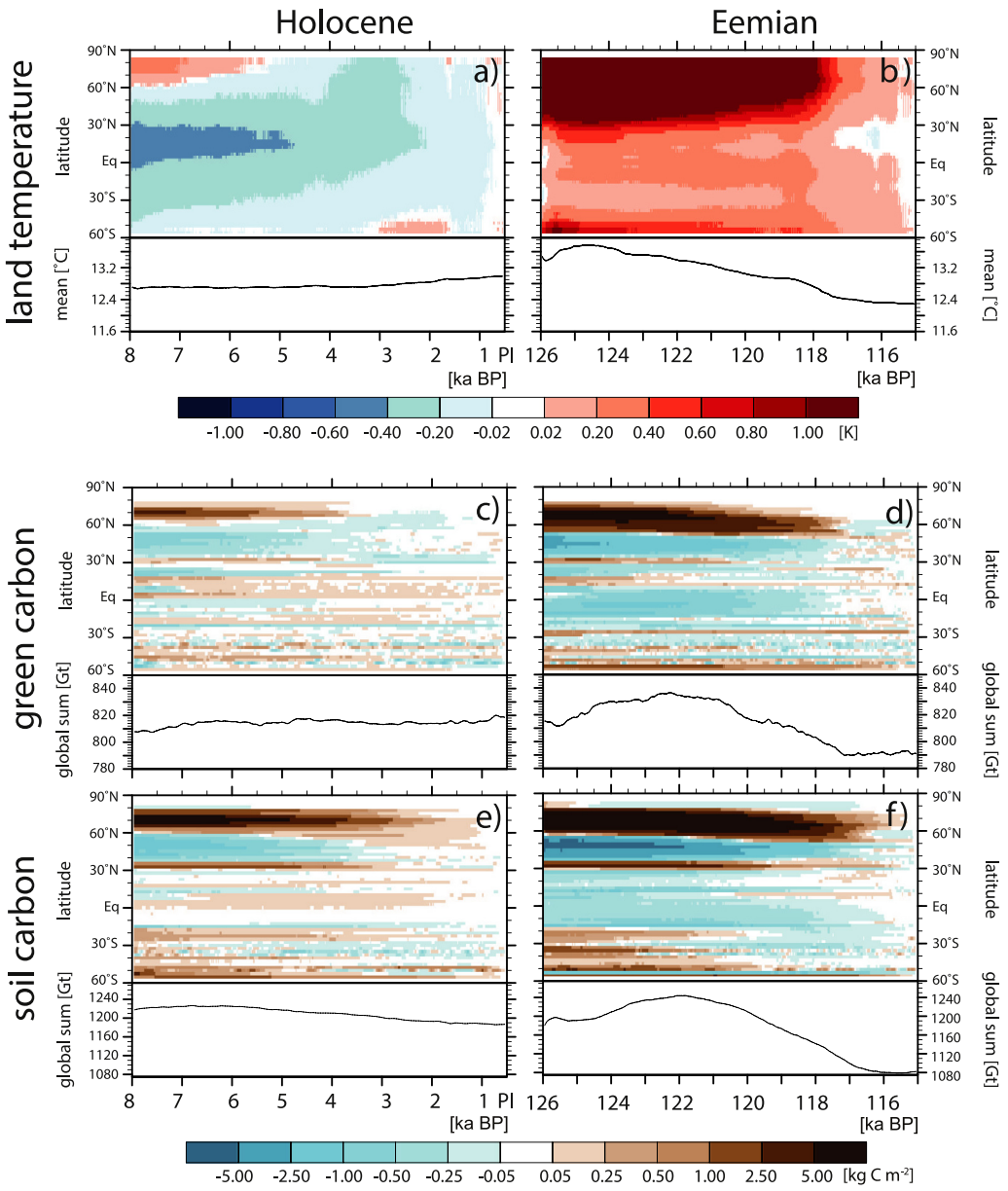


Fig. 4. Hofmöller diagrams for changes in soil carbon (kg Cm^{-2}), biomass carbon (kg Cm^{-2}) and annual mean land surface temperature (K) for the Holocene period (a, c, e) and the Eemian (b, d, f), simulated by the Bern3D model in simulations Holo_All and Eem_All, respectively. The reference period is the last 500 yrs of the simulation.

A latitudinal difference in woody cover distribution between the two interglacial periods is shown in Fig. 6. For 8 ka BP, both models have slightly higher woody (tree) cover than for present. The strongest increase in the tree cover is located in the high northern latitudes, in line with changes in terrestrial biomass. After 8 ka BP, the total woody cover decreases with time by about 300 and 100 Mha in the Bern3D and CLIMBA models, respectively. During the Eemian period, the Bern3D model shows a maximum in total woody area at 124 ka BP (Fig. 6b), about 2 thousand years earlier than a maximum in soil and biomass carbon (Fig. 4d, f). The CLIMBA model simulates continuous decrease in the woody cover during the Eemian (Fig. 7d), which is not connected to the maximum in the terrestrial carbon storage at ca. 122 ka BP (Fig. 5b, d). Summarizing the land biomass and mineral soil carbon response, the two models with terrestrial carbon components have similar patterns of response to the orbital and CO_2 changes. The magnitude of change differs mainly because of mineral soil carbon response. The change in atmospheric CO_2 concentration measured in ice cores during the Eemian is not reproduced in either of the models under the chosen simulation protocol.

4.3. Factorial experiments

4.3.1. Response to the enhanced shallow-water $CaCO_3$ sedimentation

To test the model response to shallow-water $CaCO_3$ sedimentation, we replaced the Holocene scenario of $CaCO_3$ sedimentation by Vecsei and Berger (2004) with the estimate of Opdyke and Walker (1992) of enhanced $CaCO_3$ sedimentation. The Bern3D model is most reactive to the forcing: CO_2 increases by 30 and 41 ppm during the Holocene and the Eemian experiments, respectively (Table 2, Fig. 8). Since the Eemian simulation is 40% longer, the stronger effect of $CaCO_3$ sedimentation is not surprising. The response of the CLIMBA model is much smaller (7 and 11 ppm,

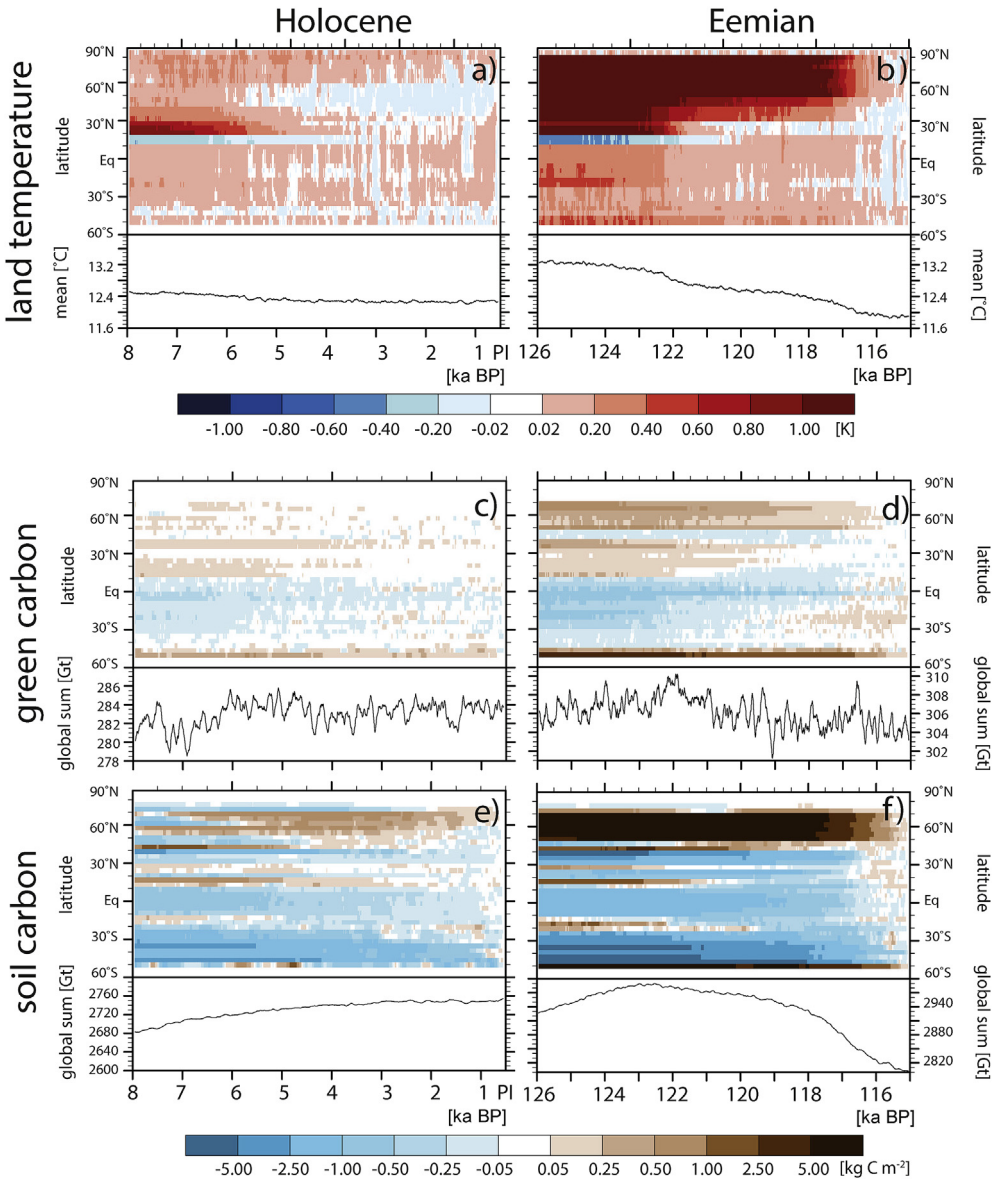


Fig. 5. The same as Fig. 4 but for the CLIMBA model.

respectively) due to differences in the marine carbonate chemistry and the land carbon uptake (with higher CO_2 levels, the terrestrial carbon uptake increases, drawing the CO_2 down). The GENIE model shows an intermediate response (20 and 25 ppm, respectively), however, this increase in CO_2 would likely be smaller if the model also accounted for terrestrial carbon uptake.

The high $CaCO_3$ accumulation of the 12 Tmol/yr in the Holo_12T experiment could easily explain the scale of the CO_2 increase in the Holocene in all models. However, if we account for the same scenario of $CaCO_3$ accumulation in the Eemian, the resulting simulated CO_2 increase in the Eem_12T experiments would exceed the already high CO_2 increase in the Eem_All simulations. These simulations therefore indicate variability among the models in terms of responses to $CaCO_3$ accumulation in the surface ocean. Global models of coral reef accumulation (Kleypas, 1997) are still very simplistic (Jones et al., 2015), and are not included in the Earth System models. This lack of shallow-water carbonate accumulation modules is a current gap in the model development for millennial-scale simulations.

Because $\delta^{13}C$ of marine carbonates is close to zero, the increase in carbonate sedimentation does not have a direct effect on $\delta^{13}CO_2$. However, there is an indirect effect on $\delta^{13}CO_2$ through changes in the atmospheric CO_2 concentration. All models show an increase in $\delta^{13}CO_2$ in the range between 0.07‰ for CLIMBA in both simulations and 0.19‰ for the Bern3D model for the Eemian experiment (Table 2). For Bern3D and CLIMBA models, this increase is explained by the terrestrial carbon increase due to CO_2 fertilization effect.

4.3.2. *Response to the peat accumulation*

The response to the peat forcing is similar among the models. In response to the accumulation of 25 GtC/ka, the models simulate a decrease in atmospheric CO_2 from 7 to 10 ppm for the Holocene and from 13 to 17 ppm for the Eemian period (Table 2, Fig. 8). Atmospheric $\delta^{13}CO_2$ increases by 0.08–0.17‰ as peat carbon has an isotopic signature close to C_3 plants and its accumulation leads to higher $\delta^{13}CO_2$ values. The response of the land biosphere counteracts the CO_2 decrease via the CO_2 fertilization mechanism where terrestrial carbon is released to the atmosphere leading to higher

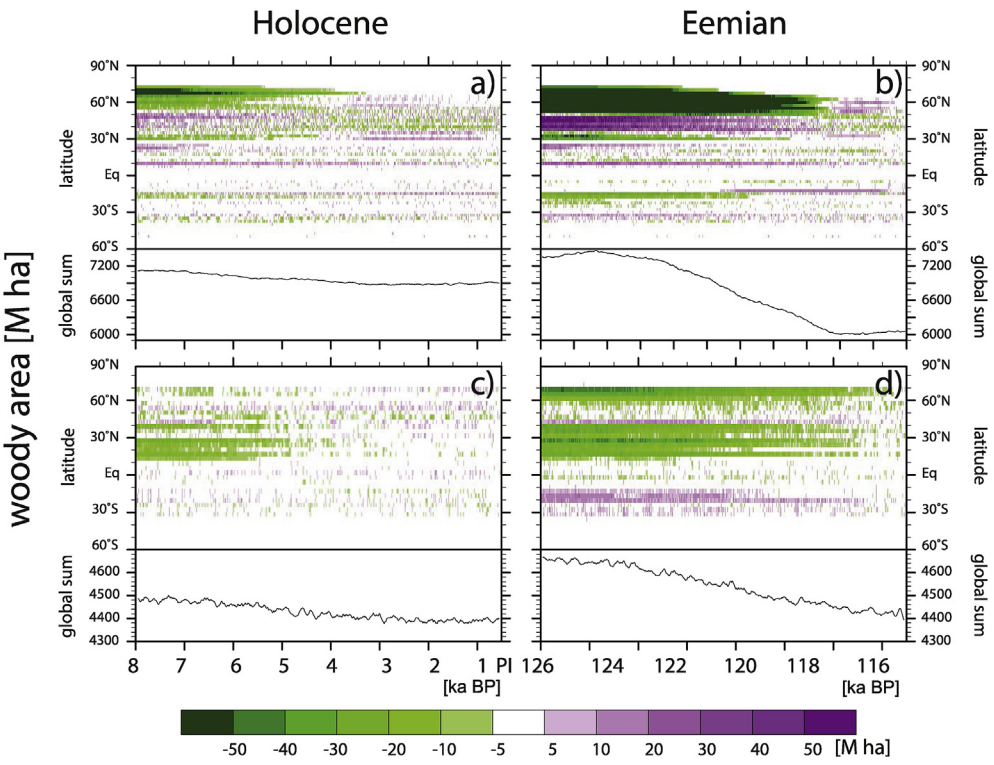


Fig. 6. Hofmöller diagrams for changes in the woody cover area (Mha) for the Holocene (a, c) and the Eemian (b, d), simulated by the Bern3D (a, b) and the CLIMBA (c, d) models in Holo_All and Eem_All, respectively. The reference period is the last 500 yrs of the simulation.

CO_2 and lower $\delta^{13}CO_2$. This combination explains the smaller response of CLIMBA relative to the Bern3D model as CLIMBA in general has a rather high CO_2 fertilization effect.

For the peat accumulation forcing, we choose a moderate peat accumulation scenario with 200 Gt carbon uptake over the last 8000 years.The estimate by Yu (2012) suggests almost two times higher accumulation in peat, while a modeling study by Kleinen et al. (2015) resulted in less peat accumulation (ca. 300 GtC) over the same period. High peat forcings are possible to accommodate in the model framework, but should then be counteracted by a strong forcing in CO_2 release due to other mechanisms. Let us note that the CO_2 release due to land use (Ruddiman, 2013) was not likely a source of CO_2 for the high peat accumulation scenario in the early Holocene due to differences in the timing and evolution of peat and land use forcings (see Section 2.2.1.4). One of the possible contributors to peat accumulation could be carbonate compensation to the pre-Holocene changes in the carbon cycle (Section 2.2.2.2) that are not considered in our experimental setup.

4.3.3. Response to the landuse emissions during the Holocene

The CO_2 and $\delta^{13}CO_2$ response strongly depends on the land use scenario. From 8 to 0.5 ka BP, total accumulated land use emissions are 26 and 167 GtC for the Holo_All and Holo_Kc scenarios, respectively. Relative to the Holo_All simulation, the Holo_Kc leads to an increase in atmospheric CO_2 by 7–11 ppm and a decrease in atmospheric $\delta^{13}CO_2$ by 0.07–0.10‰ (Table 2, Fig. 8). The effect of this scenario on CO_2 and $\delta^{13}CO_2$ is almost exactly opposite to the effect of the peat accumulation scenario due to a similar amount of carbon released or taken from the atmosphere by 0.5 ka BP. The main difference is in the timing of CO_2 change. While the peat accumulation is prescribed to increase linearly with time, more than half of the land use emissions are emitted during the period after 2 ka BP, substantially later than the CO_2 increase in the ice core data. For comparison with the Holo_Kc scenario, the HYDE scenario does not elevate the atmospheric CO_2 at 0.5 ka BP by more than 1–2 ppm in all models because of a very small amount of carbon released to the atmosphere.

In our simulations, changes in land use and land cover result in an increase of atmospheric CO_2 up to 11 ppm in the period between 8 and 0.5 ka BP. It is difficult to judge the plausibility of these changes, as all applied scenarios are based on the hypothesis of human population development and not on an objective reconstruction of land cover change. The reconstruction of landuse changes via changes in pollen assemblages is a promising approach, but the current state of data synthesis still requires many years in order to have a reliable quantitative estimate of global tree cover changes over the last 8000 years. Furthermore, changes in soil carbon as well as permafrost carbon storage would still remain unaccounted for. There is no doubt that anthropogenic and land cover changes have contributed to the changes in the atmospheric CO_2 during the Holocene, but it is more likely that this effect only became visible during the last 3000 years.

4.3.4. Response to the SST changes

We used simulations Holo_noO and Eem_noO without orbital forcing performed with the GENIE model to reveal the effect of SST changes. The GENIE model does not include the terrestrial carbon cycle, and therefore a difference in atmospheric CO_2 and $\delta^{13}CO_2$ between simulations with and without orbital forcing could be attributed to changes in SSTs for the Holocene and Eemian (Table 2). For the Holocene, the GENIE model does not reveal significant changes, in line with previous model studies (Section 2.2.2.1). For the period from 126 to 115 ka BP, CO_2 and $\delta^{13}CO_2$ slightly increase by 4 ppm and 0.03‰, respectively, due to SST changes (Table 2).

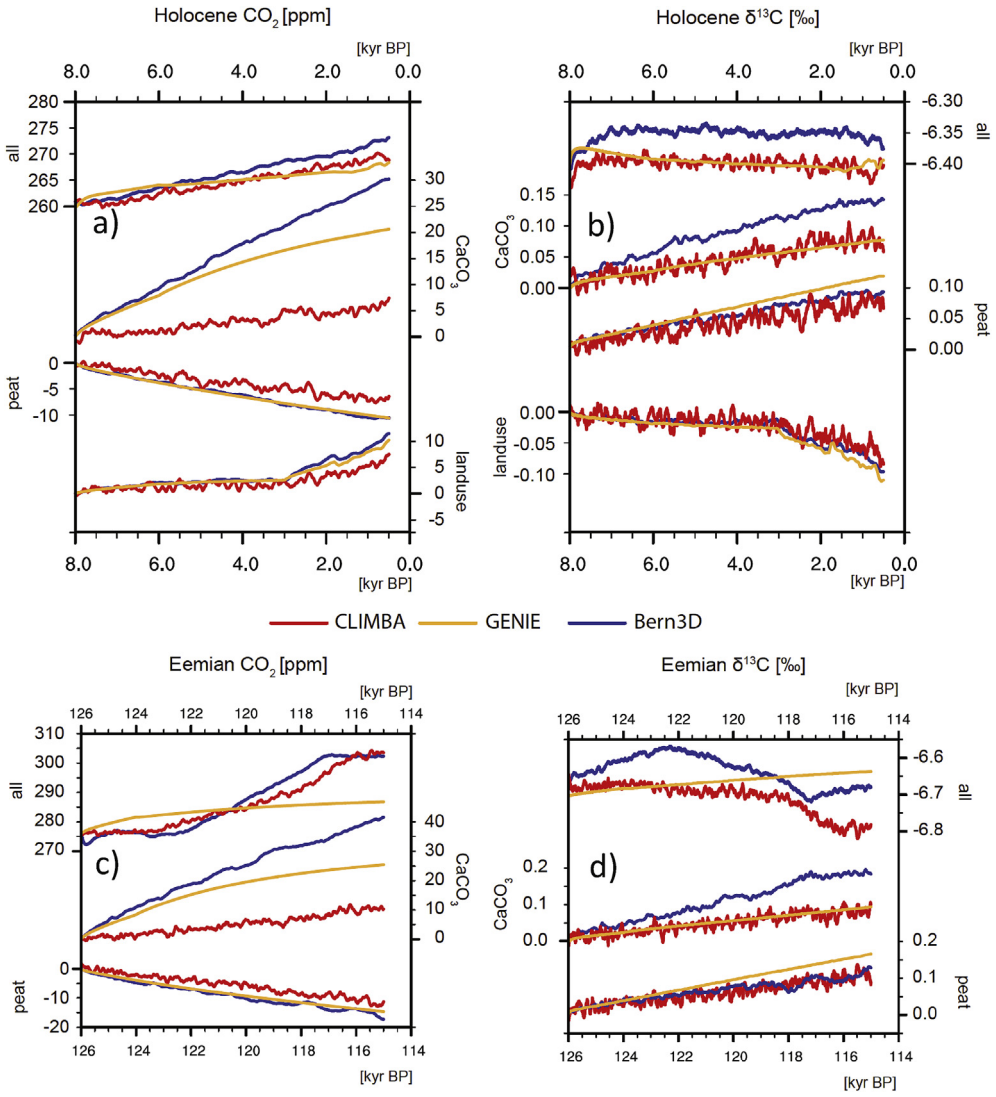


Fig. 7. Time series of simulated differences in CO_2, ppm (a, c) and $\delta^{13}CO_2$, ‰ (b, d) in response to the $CaCO_3$ sedimentation, peat, and landuse forcings for the present (a, b) and last (c, d) interglacial (see Table 2 for details). At the top of each plot, absolute values of simulated CO_2 or $\delta^{13}CO_2$ in the Holo_All and Eem_All experiments are provided as a reference.

Table 2
Simulated CO_2 and $\delta^{13}CO_2$ changes during interglacials (200-yr average).

Factor (simulation difference)	Model		
	Bern-3D	CLIMBA	GENIE
Holocene (8–0.5 ka)			
SSTs (Holo_All − Holo_noO)	–	–	0/0.01
$CaCO_3$ sedimentation (Holo_12T− Holo_All)	30/0.14[a]	7/0.07	20/0.08
Peat accumulation (Holo_P − Holo_All)	−10/0.09	−7/0.08	−10/0.12
Landuse (Holo_Kc − Holo_All)	11/−0.09	7/−0.07	9/−0.10
Eemian (126–115 ka)			
SSTs (Eem_All − Eem_noO)	–	–	4/0.03
$CaCO_3$ sedimentation (Eem_12T − Eem_All)	41/0.19	11/0.08	25/0.09
CO_2 fertilization, biome shifts & wildfires[b]	7/−0.06	6/−0.05	–
Peat accumulation (Eem_P − Eem_All)	−17/0.13	−13/0.1	−15/0.17

[a] CO_2 changes in ppm/$\delta^{13}CO_2$ changes in ‰
[b] Based on land carbon changes in Eem_All.

4.4. Summary of interglacial carbon cycle processes

A summary of effects of interglacial carbon cycle processes on atmospheric CO_2 and $\delta^{13}CO_2$ is presented in Fig. 8. Black (gray) dots indicate process-attributed changes found in this (previous) study, while averaged increase (decrease) in all studies is presented by red (blue) bars. For the ice core data, averaged changes over the analyzed interval are presented by yellow bars, and black dots with whiskers indicate the ±1σ uncertainty interval (Fig. 1). Processes are subdivided into marine (SSTs, coral reef and carbonate compensation) and terrestrial (CO_2 fertilization, biome shifts and wildfires, peat accumulation and landuse) mechanisms following the experimental setup. Changes in SSTs have small effects on the carbon cycle (0–4 ppm) during both interglacials (black dots indicate the GENIE model results). Coral reefs and carbonate compensation contribute strongly to the CO_2 increase during both interglacials (7–41 ppm), while peat accumulation leads to a strong decrease in CO_2 (7–17 ppm). The CO_2 fertilization and biome shifts mechanisms operate differently during the Holocene and Eemian. While the natural vegetation is likely a sink for carbon due to increasing CO_2 during the Holocene, the land biosphere is a source of carbon due to biome shifts in response to climate change during the Eemian (6–7 ppm increase in CO_2). Landuse is a source of carbon to the atmosphere at the end of the Holocene (7–11 ppm).

Changes in terrestrial carbon storages due to CO_2 fertilization

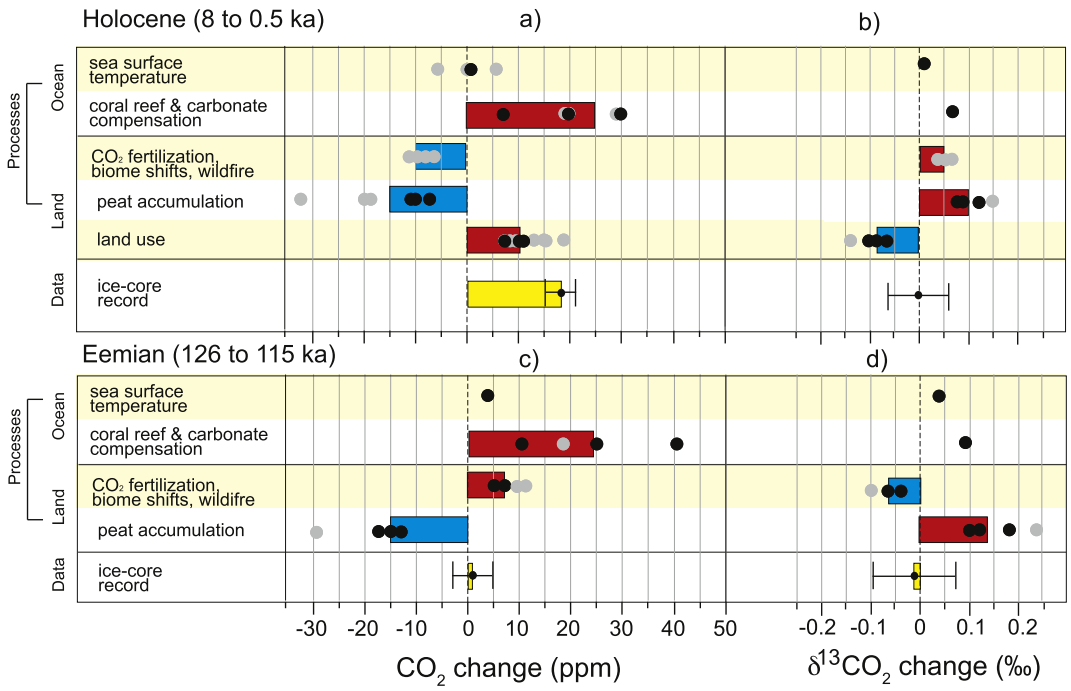


Fig. 8. Relative contributions of different processes to changes in atmospheric CO_2 concentration, ppm (a, c) and $\delta^{13}CO_2$, ‰ (b, d) during the Holocene (a, b) and the Eemian (c, d). Gray dots are for previous studies incl. (Kleinen et al., 2015) while black dots and uncertainty ranges are for the given study. After Fig. 6.5 in Ciais et al. (2013) modified from Kohfeld and Ridgwell (2009).

and peat accumulation are mirrored in the left and right parts of Fig. 8: when land takes carbon, atmospheric CO_2 decreases (blue bar) while $\delta^{13}CO_2$ increases (red bar), and vice versa. The coral reef and carbonate compensation mechanisms significantly change atmospheric CO_2, but their direct effect on $\delta^{13}CO_2$ is very small because the $\delta^{13}C$ signature of $CaCO_3$ fluxes is close to zero. However, there is an indirect effect in our experimental setup as land takes carbon due to fertilization effect of coral-induced CO_2 flux. This effect leads to an increase in atmospheric $\delta^{13}CO_2$ in the enhanced $CaCO_3$ sedimentation experiments in the models (Table 2). To avoid a wrong impression that coral reef accumulation could significantly influence $\delta^{13}CO_2$, we do not show color bars for coral reef effects on $\delta^{13}CO_2$. For the CO_2 fertilization effect on $\delta^{13}CO_2$ for the Holocene, we take existing studies on CO_2 and transform them to $\delta^{13}CO_2$ using sensitivity of the Holocene experiments with peatlands (−0.008‰/ppm). For the CO_2 fertilization effect on $\delta^{13}CO_2$ during the Eemian, we take the difference between 126 and 115 ka in terrestrial carbon storages in the Eem_all experiment in Bern3D and CLIMBA and use a sensitivity of Eemian experiments with peatlands (−0.007‰/ppm). For landuse effect on $\delta^{13}CO_2$ in the Holocene, we use the model results from Table 2.

Ideally, if models were able to capture all important carbon cycle processes and these processes were independent from each other, the sum of blue and red bars on Fig. 8 should be equal to the ice core data represented by yellow bars for each particular period for each variable. This linear approach underestimates non-linear interactions between carbon cycle processes, but it is useful for a visual comparison of significance and direction of changes due to particular mechanism and for illustrating the point whether all relevant components are accounted for. This linear approach is approximately correct for the Holocene changes in CO_2, but not valid for the Eemian as CO_2 sources (sum of red bars) are higher than the CO_2 sinks (blue bar). As discussed above, this difference could be due to overestimation of the coral reef accumulation or due to a wrong terrestrial biosphere response to the cooling at the end of the Eemian. For the ^{13}C budget, models project increases in $\delta^{13}CO_2$ during both the Holocene and Eemian while data show no change. Although modeled $\delta^{13}CO_2$ increase is within the 1σ-uncertainty envelope of measurements, it is possible that models miss a source of light carbon to the atmosphere towards the end of the Holocene and overestimate release of biospheric carbon to the atmosphere during the 2nd part of the Eemian.

5. Conclusions

By applying exactly the same set of forcings to the Holocene and Eemian period, we compare the significance of the responsible processes on the carbon cycle during these two interglacials. We are able to qualitatively (and not yet quantitatively) explain CO_2 and $\delta^{13}CO_2$ dynamics for the Holocene as a result of several counteracting mechanisms: $CaCO_3$ accumulation in shallow waters, changes in natural terrestrial carbon, and anthropogenic landuse emissions in the later part of the Holocene. However, when we use the same set of forcings (excluding landuse) for the Eemian period, the direction of changes in atmospheric CO_2 concentration after 121 ka BP is the opposite of the reconstructed changes. This discrepancy could be explained by rather unrealistic assumptions about the carbon cycle forcings in the Eemian, or by the inability of terrestrial carbon models to simulate proper responses to the cooling during the end of interglacial periods.

Ice-core records of atmospheric $\delta^{13}CO_2$ show very similar values at 8 and 0.5 ka BP and at 126 and 115 ka BP (Figs. 1 and 8). Mechanisms of marine ^{13}C fractionation (Broecker and McGee, 2013) such as changes in fractionation at the ocean-atmosphere boundary and marine photosynthesis are included in our simulations, yet they do not affect atmospheric $\delta^{13}CO_2$ in the Holocene. SSTs in convective areas in polar regions with strong exchange between the surface and the deep ocean remain unchanged throughout these time periods. The change in the marine biological pump (Goodwin et al., 2011) could shift the atmospheric $\delta^{13}CO_2$, but there

is no clear support for such a change in the marine proxies for biological productivity. Therefore, the main interpretation of atmospheric $\delta^{13}CO_2$ is linked to changes in the terrestrial biosphere, particularly in storage in mineral soils, peat, and permafrost carbon. Let us note that the mechanisms responsible for the 0.3‰ offset in atmospheric $\delta^{13}CO_2$ between the Holocene and Eemian (Fig. 1) could not be identified with our experimental setup.

Terrestrial models used in this study show similar patterns of land carbon and vegetation changes during both the Holocene and Eemian. The main changes in terrestrial carbon storage occur in the northern high latitudes. The amplitude of changes is much stronger in the Eemian than in the Holocene. This difference is in general agreement with available pollen records. However, the current generation of land carbon models does not incorporate processes of carbon accumulation and decay in anaerobic and permafrost environments, although, for the latter, specific permafrost modules adapted to EMICs may soon be available (Crichton et al., 2014). In response to the onset of cooling in the high northern latitudes in the Eemian, models simulate a southward retreat of boreal forests (in line with the data) and a loss of carbon from these regions. The latter is unrealistic if one accounts for the ability of the permafrost environment to accumulate soil carbon in frozen form for many millennia. Global models of the permafrost carbon and peat dynamics were recently developed (e.g.,Spahni et al., 2013; Stocker et al., 2014), as the ESM ability to simulate the carbon dynamics in high latitudes is important not only for the past but also for the future (Schuur et al., 2013).

Simulations in this study assumed constant accumulation of $CaCO_3$ in shallow waters. This assumption is a strong simplification because coral productivity depends on many factors including changes in temperature, nutrients, and sea level. The models currently used for coral reef growth on a global scale (e.g., Kleypas, 1997) are developed as steady-state approximations. Accounting for the transient dynamics of coral reef growth will change the model results and lead to a more plausible effect on atmospheric CO_2, in particular, towards the end of the Eemian. The development of reliable models of coral reef growth will improve the ability of ESMs to simulate long-term dynamics of marine carbonate chemistry during warm intervals.

Because the peak in landuse emissions is shifted towards the end of the Holocene, the landuse forcing does not help in explaining the CO_2 growth prior to 2–3 ka BP. Nonetheless, a large spread in the amplitude of landuse emissions is one of the major sources of uncertainties in simulations of CO_2 dynamics during the Holocene. The high-end emission scenarios such as by Kaplan et al. (2011) require large areas of conversion from forests to open landscapes, which should also be present in the pollen records. Therefore, there is a need in large-scale reconstruction of landuse and land cover changes based on the dynamics of pollen assemblage (Fyfe et al., 2015; Gaillard et al., 2010). Charcoal synthesis data is another useful archive for reconstructing the scale of landuse changes. A simplified version of wildfire activity is included in the JSBACH model (Bruecher et al., 2014), but it does not show a strong trend in burned areas during the Holocene or Eemian.

In this study, we performed experiments with a limited number of carbon cycle forcings. While some processes, such as changes in the marine biological pump and sea surface temperatures, are explicitly included in the simulations, some mechanisms remain completely untouched. In particular, numerical approaches to model global volcanic CO_2 emissions and methane hydrate storages are still in their infancy. The current uncertainties associated with these processes may be reduced using isotopic constraints but the level of confidence in the role of these forcings will remain low until we better understand their long-term dynamics. Another limitation of our experiments was an assumption of equilibrium initial conditions. Therefore, we neglected memory (legacy) effects arising from changes over previous terminations. These non-equilibrium effects could be studied in long-term transient simulations of deglaciations or complete glacial cycles, which are still beyond computational abilities of most of ESMs.

Last but not least, the models used in this study are rather simple in comparison with state-of-the-art ESMs, but these models provide a prototype for long-term experiments with more comprehensive models and demonstrate the main uncertainties in the of CO_2 forcings during interglacials. Model deficiencies identified here will stimulate model development useful not only for simulating past climates, but also for more reliable projections of future carbon cycle changes and climate dynamics.

Author contributions

V.B. coordinated manuscript writing. V.B., T. Brücher, and R.R. designed the experimental setup. T. Brücher performed simulations of the CLIMBA model and prepared Figs. 2–7 with intercomparison of the model results. S.Z. contributed to the JSBACH model version used in the CLIMBA model. R.R., F.J., and R.S. performed simulations of the Bern3D model, E.S. and A.R. provided results of the GENIE model. J.S., H.F. and M.L. provided Fig. 1 and discussed implications of the CO_2 and $\delta^{13}CO_2$ measurements in the ice cores. N.K., T.K., and R.S. contributed with the overview sections on the fire, peat, and permafrost, respectively. All authors contributed to writing the manuscript.

Acknowledgements

The authors thank Laurent Bopp for providing prototype of Fig. 8. We are grateful to two anonymous reviewers for their useful and constructive comments. The research leading to these results has received funding from the European Union's Seventh Framework programme (FP7/2007–2013) under grant agreement no 243908, "Past4Future. Climate change - Learning from the past climate". The division for Climate and Environmental Physics, University of Bern, acknowledges long-term financial support by the Swiss National Science Foundation. This is Past4Future contribution no 88.

Appendix A. Supplementary data

Supplementary data related to this article can be found at http://dx.doi.org/10.1016/j.quascirev.2016.01.028

References

Ainsworth, E.A., Rogers, A., 2007. The response of photosynthesis and stomatal conductance to rising CO_2 : mechanisms and environmental interactions. Plant Cell Environ. 30, 258–270.
Anderson, R.F., Fleisher, M.Q., Lao, Y., Winckler, G., 2008. Modern $CaCO_3$ preservation in equatorial Pacific sediments in the context of late-Pleistocene glacial cycles. Mar. Chem. 111, 30–46.
Anthony, K.M.W., Zimov, S.A., Grosse, G., Jones, M.C., Anthony, P.M., Chapin, F.S., Finlay, J.C., Mack, M.C., Davydov, S., Frenzel, P., Frolking, S., 2014. A shift of thermokarst lakes from carbon sources to sinks during the Holocene epoch. Nature 511, 452-+.
Archer, D., 1996. A data-driven model of the global calcite lysocline. Glob. Biogeochem. Cycles 10, 511–526.
Archer, D., Buffett, B., Brovkin, V., 2009. Ocean methane hydrates as a slow tipping point in the global carbon cycle. Proc. Natl. Acad. Sci. 106, 20596–20601.
Archer, D., Martin, P., Buffett, B., Brovkin, V., Rahmstorf, S., Ganopolski, A., 2004. The importance of ocean temperature to global biogeochemistry. Earth Planet. Sci. Lett. 222, 333–348.
Barnola, J.M., Raynaud, D., Korotkevich, Y.S., Lorius, C., 1987. Vostok ice core provides 160,000-year record of atmospheric CO_2. Nature 329, 408–414.
Bauska, T.K., Joos, F., Mix, A.C., Roth, R., Ahn, J., Brook, E.J., 2015. Links between atmospheric carbon dioxide, the land carbon reservoir and climate over the past millennium. Nat. Geosci. 8, 383–387.

Berger, A., Loutre, M.F., 1991. Insolation values for the climate of the last 10,000,000 years. Quat. Sci. Rev. 10, 297–317.
Bock, M., Schmitt, J., Moller, L., Spahni, R., Blunier, T., Fischer, H., 2010. Hydrogen isotopes preclude Marine hydrate CH_4 emissions at the onset of Dansgaard-Oeschger events. Science 328, 1686–1689.
Bowman, D., Balch, J.K., Artaxo, P., Bond, W.J., Carlson, J.M., Cochrane, M.A., D'Antonio, C.M., DeFries, R.S., Doyle, J.C., Harrison, S.P., Johnston, F.H., Keeley, J.E., Krawchuk, M.A., Kull, C.A., Marston, J.B., Moritz, M.A., Prentice, I.C., Roos, C.I., Scott, A.C., Swetnam, T.W., van der Werf, G.R., Pyne, S.J., 2009. Fire in the earth system. Science 324, 481–484.
Broecker, W.S., Clark, E., McCorkle, D.C., Peng, T.H., Hajdas, I., Bonani, G., 1999. Evidence for a reduction in the carbonate ion content of the deep sea during the course of the Holocene. Paleoceanography 14, 744–752.
Broecker, W.S., Lynch-Stieglitz, J., Clark, E., Hajdas, I., Bonani, G., 2001. What caused the atmosphere's CO2 content to rise during the last 8000 years? Geochem. Geophys. Geosyst. 2 art. no.-2001GC000177.
Broecker, W.S., McGee, D., 2013. The C-13 record for atmospheric CO_2: what is it trying to tell us? Earth Planet. Sci. Lett. 368, 175–182.
Brovkin, V., Bendtsen, J., Claussen, M., Ganopolski, A., Kubatzki, C., Petoukhov, V., Andreev, A., 2002. Carbon cycle, vegetation, and climate dynamics in the Holocene: experiments with the CLIMBER-2 model. Glob. Biogeochem. Cycles 16.
Brovkin, V., Ganopolski, A., Archer, D., Munhoven, G., 2012. Glacial CO_2 cycle as a succession of key physical and biogeochemical processes. Clim. Past 8, 251–264.
Brovkin, V., Kim, J.H., Hofmann, M., Schneider, R., 2008. A lowering effect of reconstructed Holocene changes in sea surface temperatures on the atmospheric CO_2 concentration. Glob. Biogeochem. Cycles 22.
Brovkin, V., Raddatz, T., Reick, C.H., Claussen, M., Gayler, V., 2009. Global biogeophysical interactions between forest and climate. Geophys. Res. Lett. 36.
Brovkin, V., Sitch, S., von Bloh, W., Claussen, M., Bauer, E., Cramer, W., 2004. Role of land cover changes for atmospheric CO_2 increase and climate change during the last 150 years. Glob. Change Biol. 10, 1253–1266.
Bruecher, T., Brovkin, V., Kloster, S., Marlon, J.R., Power, M.J., 2014. Comparing modelled fire dynamics with charcoal records for the Holocene. Clim. Past 10, 811–824.
Burton, M.R., Sawyer, G.M., Granieri, D., 2013. Deep carbon emissions from volcanoes. In: Hazen, R.M., Jones, A.P., Baross, J.A. (Eds.), Carbon in Earth, pp. 323–354.
Chikamoto, M.O., Matsumoto, K., Ridgwell, A., 2008. Response of deep-sea CaCO3 sedimentation to Atlantic meridional overturning circulation shutdown. J. Geophys. Res. 113, G03017. http://dx.doi.org/10.1029/2007JG000669.
Ciais, P., Sabine, C., Bala, G., Bopp, L., Brovkin, V., Canadell, J., Chhabra, A., DeFries, R., Galloway, J., Heimann, M., Jones, C., Le Quéré, C., Myneni, R.B., Piao, S., Thornton, P., 2013. Carbon and other biogeochemical cycles. In: Stocker, T.F., Qin, D., Plattner, G.-K., Tignor, M., Allen, S.K., Boschung, J., Nauels, A., Xia, Y., Bex, V., Midgley, P.M. (Eds.), Climate Change 2013: the Physical Science Basis. Contribution of Working Group I to the Fifth Assessment Report of the Intergovernmental Panel on Climate Change Cambridge University Press, Cambridge, United Kingdom and New York, NY, USA.
Ciais, P., Tagliabue, A., Cuntz, M., Bopp, L., Scholze, M., Hoffmann, G., Lourantou, A., Harrison, S.P., Prentice, I.C., Kelley, D.I., Koven, C., Piao, S.L., 2012. Large inert carbon pool in the terrestrial biosphere during the last glacial maximum. Nat. Geosci. 5, 74–79.
Colbourn, G., Ridgwell, A., Lenton, T.M., 2013. The Rock Geochemical Model (RokGeM) v0.9. Geosci Model Dev. 6, 1543–1573. http://dx.doi.org/10.5194/gmd-6-1543-2013.
Cramer, W., Bondeau, A., Woodward, F.I., Prentice, I.C., Betts, R.A., Brovkin, V., Cox, P.M., Fisher, V., Foley, J.A., Friend, A.D., Kucharik, C., Lomas, M.R., Ramankutty, N., Sitch, S., Smith, B., White, A., Young-Molling, C., 2001. Global response of terrestrial ecosystem structure and function to CO_2 and climate change: results from six dynamic global vegetation models. Glob. Change Biol. 7, 357–373.
Crichton, K., Roche, D., Krinner, G., Chappellaz, J., 2014. A simplified permafrost-carbon model for long-term climate studies with the CLIMBER-2 coupled earth system model. Geosci. Model Dev. 7, 3111–3134.
De Kauwe, M.G., Medlyn, B.E., Zaehle, S., Walker, A.P., Dietze, M.C., Wang, Y.P., Luo, Y.Q., Jain, A.K., El-Masri, B., Hickler, T., Warlind, D., Weng, E.S., Parton, W.J., Thornton, P.E., Wang, S.S., Prentice, I.C., Asao, S., Smith, B., McCarthy, H.R., Iversen, C.M., Hanson, P.J., Warren, J.M., Oren, R., Norby, R.J., 2014. Where does the carbon go? a model-data intercomparison of vegetation carbon allocation and turnover processes at two temperate forest free-air CO_2 enrichment sites. New Phytol. 203, 883–899.
Dommain, R., Couwenberg, J., Glaser, P.H., Joosten, H., Nyoman, I., Suryadiputra, N., 2014. Carbon storage and release in Indonesian peatlands since the last deglaciation. Quat. Sci. Rev. 97, 1–32.
Edwards, N., Marsh, R., 2005. Uncertainties due to transport-parameter sensitivity in an efficient 3-D ocean-climate model. Clim. Dyn. 24, 415–433.
Elsig, J., Schmitt, J., Leuenberger, D., Schneider, R., Eyer, M., Leuenberger, M., Joos, F., Fischer, H., Stocker, T.F., 2009. Stable isotope constraints on Holocene carbon cycle changes from an Antarctic ice core. Nature 461, 507–510.
Farrell, J.W., Prell, W.L., 1989. Climatic change and $CaCO_3$ preservation: an 800,000 year bathymetric reconstruction from the central equatorial Pacific Ocean. Paleoceanography 4, 447–466.
Ferretti, D.F., Miller, J.B., White, J.W.C., Etheridge, D.M., Lassey, K.R., Lowe, D.C., Meure, C.M.M., Dreier, M.F., Trudinger, C.M., van Ommen, T.D., Langenfelds, R.L., 2005. Unexpected changes to the global methane budget over the past 2000 years. Science 309, 1714–1717.
Flannigan, M.D., Krawchuk, M.A., de Groot, W.J., Wotton, B.M., Gowman, L.M., 2009. Implications of changing climate for global wildland fire. Int. J. Wildland Fire 18, 483–507.
Foley, J.A., 1994. The sensitivity of the terrestrial biosphere to climatic change – a simulation of the middle Holocene. Glob. Biogeochem. Cycles 8, 505–525.
Fyfe, R.M., Woodbridge, J., Roberts, N., 2015. From forest to farmland: pollen-inferred land cover change across Europe using the pseudobiomization approach. Glob. Change Biol. 21, 1197–1212.
Gaillard, M.J., Sugita, S., Mazier, F., Trondman, A.K., Brostrom, A., Hickler, T., Kaplan, J.O., Kjellstrom, E., Kokfelt, U., Kunes, P., Lemmen, C., Miller, P., Olofsson, J., Poska, A., Rundgren, M., Smith, B., Strandberg, G., Fyfe, R., Nielsen, A.B., Alenius, T., Balakauskas, L., Barnekow, L., Birks, H.J.B., Bjune, A., Bjorkman, L., Giesecke, T., Hjelle, K., Kalnina, L., Kangur, M., van der Knaap, W.O., Koff, T., Lageras, P., Latalowa, M., Leydet, M., Lechterbeck, J., Lindbladh, M., Odgaard, B., Peglar, S., Segerstrom, U., von Stedingk, H., Seppa, H., 2010. Holocene land-cover reconstructions for studies on land cover-climate feedbacks. Clim. Past 6, 483–499.
Ganopolski, A., Petoukhov, V., Rahmstorf, S., Brovkin, V., Claussen, M., Eliseev, A., Kubatzki, C., 2001. CLIMBER-2: a climate system model of intermediate complexity. Part II: model sensitivity. Clim. Dyn. 17, 735–751.
Gerlach, T., 2011. Volcanic versus anthropogenic carbon dioxide. Eos, Trans. Am. Geophys. Union 92, 201–202.
Giorgetta, M.A., Jungclaus, J., Reick, C.H., Legutke, S., Bader, J., Boettinger, M., Brovkin, V., Crueger, T., Esch, M., Fieg, K., Glushak, K., Gayler, V., Haak, H., Hollweg, H.-D., Ilyina, T., Kinne, S., Kornblueh, L., Matei, D., Mauritsen, T., Mikolajewicz, U., Mueller, W., Notz, D., Pithan, F., Raddatz, T., Rast, S., Redler, R., Roeckner, E., Schmidt, H., Schnur, R., Segschneider, J., Six, K.D., Stockhause, M., Timmreck, C., Wegner, J., Widmann, H., Wieners, K.-H., Claussen, M., Marotzke, J., Stevens, B., 2013. Climate and carbon cycle changes from 1850 to 2100 in MPI-ESM simulations for the coupled model intercomparison Project phase 5. J. Adv. Model. Earth Syst. 5, 572–597.
Goldewijk, K.K., Beusen, A., van Drecht, G., de Vos, M., 2011. The HYDE 3.1 spatially explicit database of human-induced global land-use change over the past 12,000 years. Glob. Ecol. Biogeogr. 20, 73–86.
Goodwin, P., Oliver, K.I.C., Lenton, T.M., 2011. Observational constraints on the causes of Holocene CO_2 change. Glob. Biogeochem. Cycles 25.
Hickler, T., Smith, B., Prentice, I.C., Mjofors, K., Miller, P., Arneth, A., Sykes, M.T., 2008. CO(2) fertilization in temperate FACE experiments not representative of boreal and tropical forests. Glob. Change Biol. 14, 1531–1542.
Hugelius, G., Strauss, J., Zubrzycki, S., Harden, J.W., Schuur, E., Ping, C.-L., Schirrmeister, L., Grosse, G., Michaelson, G., Koven, C., 2014. Improved estimates show large circumpolar stocks of permafrost carbon while quantifying substantial uncertainty ranges and identifying remaining data gaps. Biogeosci. Discuss. 11, 4771–4822.
Huybers, P., Langmuir, C., 2009. Feedback between deglaciation, volcanism, and atmospheric CO_2. Earth Planet. Sci. Lett. 286, 479–491.
Indermühle, A., Stocker, T.F., Joos, F., Fischer, H., Smith, H.J., Wahlen, M., Deck, B., Mastroianni, D., Tschumi, J., Blunier, T., Meyer, R., Stauffer, B., 1999. Holocene carbon-cycle dynamics based on CO_2 trapped in ice at Taylor Dome, Antarctica. Nature 398, 121–126.
Jones, N.S., Ridgwell, A., Hendy, E.J., 2015. Evaluation of coral reef carbonate production models at a global scale. Biogeosciences 12, 1339–1356. http://dx.doi.org/10.5194/bg-12-1339-2015.
Joos, F., Gerber, S., Prentice, I.C., Otto-Bliesner, B.L., Valdes, P.J., 2004. Transient simulations of Holocene atmospheric carbon dioxide and terrestrial carbon since the last glacial maximum. Glob. Biogeochem. Cycles 18.
Kaplan, J.O., Krumhardt, K.M., Ellis, E.C., Ruddiman, W., Klein Goldewijk, K., 2011. Holocene carbon emissions as a result of anthropogenic land cover change. Holocene 21 (5), 775–791.
Kaplan, J.O., Krumhardt, K.M., Zimmermann, N., 2009. The prehistoric and preindustrial deforestation of Europe. Quat. Sci. Rev. 28, 3016–3034.
Kaplan, J.O., Prentice, I.C., Knorr, W., Valdes, P.J., 2002. Modeling the dynamics of terrestrial carbon storage since the last glacial maximum. Geophys. Res. Lett. 29.
Kim, J.H., Rimbu, N., Lorenz, S.J., Lohmann, G., Nam, S.I., Schouten, S., Ruhlemann, C., Schneider, R.R., 2004. North Pacific and North Atlantic sea-surface temperature variability during the holocene. Quat. Sci. Rev. 23, 2141–2154.
Kleinen, T., Brovkin, V., Munhoven, G., 2015. Carbon cycle dynamics during recent interglacials. Clim. Past. Discuss. 11, 1945–1983.
Kleinen, T., Brovkin, V., Schuldt, R.J., 2012. A dynamic model of wetland extent and peat accumulation: results for the Holocene. Biogeosciences 9, 235–248.
Kleinen, T., Brovkin, V., von Bloh, W., Archer, D., Munhoven, G., 2010. Holocene carbon cycle dynamics. Geophys. Res. Lett. 37.
Kleinen, T., Tarasov, P., Brovkin, V., Andreev, A., Stebich, M., 2011. Comparison of modeled and reconstructed changes in forest cover through the past 8000 years: Eurasian perspective. Holocene 21, 723–734.
Kleypas, J.A., 1997. Modeled estimates of global reef habitat and carbonate production since the last glacial maximum. Paleoceanography 12, 533–545.
Kloster, S., Brücher, T., Brovkin, V., Wilkenskjeld, S., 2015. Controls on fire activity over the Holocene. Clim. Past 11, 781–788.
Kohfeld, K.E., Ridgwell, A., 2009. Glacial-interglacial variability in atmospheric CO_2. In: Le Quéré, C., Saltzman, E. (Eds.), Surface Ocean/Lower Atmosphere Processes, Geophysical Monograph Series, vol. 37. American Geophysical Union, Washington, DC.

Lloyd, J., Farquhar, G.D., 1994. C13 discrimination during CO_2 assimilation by the terrestrial biosphere. Oecologia 99, 201–215.
Lohmann, G., Pfeiffer, M., Laepple, T., Leduc, G., Kim, J.H., 2013. A model-data comparison of the Holocene global sea surface temperature evolution. Clim. Past 9, 1807–1839.
Loisel, J., Garneau, M., Helie, J.-F., 2009. Modern Sphagnum delta C-13 signatures follow a surface moisture gradient in two boreal peat bogs, James Bay lowlands, Quebec. J. Quat. Sci. 24, 209–214.
Loisel, J., Yu, Z.C., Beilman, D.W., Camill, P., Alm, J., Amesbury, M.J., Anderson, D., Andersson, S., Bochicchio, C., Barber, K., Belyea, L.R., Bunbury, J., Chambers, F.M., Charman, D.J., De Vleeschouwer, F., Fialkiewicz-Koziel, B., Finkelstein, S.A., Galka, M., Garneau, M., Hammarlund, D., Hinchcliffe, W., Holmquist, J., Hughes, P., Jones, M.C., Klein, E.S., Kokfelt, U., Korhola, A., Kuhry, P., Lamarre, A., Lamentowicz, M., Large, D., Lavoie, M., MacDonald, G., Magnan, G., Makila, M., Mallon, G., Mathijssen, P., Mauquoy, D., McCarroll, J., Moore, T.R., Nichols, J., O'Reilly, B., Oksanen, P., Packalen, M., Peteet, D., Richard, P.J.H., Robinson, S., Ronkainen, T., Rundgren, M., Sannel, A.B.K., Tarnocai, C., Thom, T., Tuittila, E.S., Turetsky, M., Valiranta, M., van der Linden, M., van Geel, B., van Bellen, S., Vitt, D., Zhao, Y., Zhou, W.J., 2014. A database and synthesis of northern peatland soil properties and Holocene carbon and nitrogen accumulation. Holocene 24, 1028–1042.
Lourantou, A., Chappellaz, J., Barnola, J.M., Masson-Delmotte, V., Raynaud, D., 2010. Changes in atmospheric CO2 and its carbon isotopic ratio during the penultimate deglaciation. Quat. Sci. Rev. 29, 1983–1992.
MacDonald, G.M., Beilman, D.W., Kremenetski, K.V., Sheng, Y.W., Smith, L.C., Velichko, A.A., 2006. Rapid early development of circumarctic peatlands and atmospheric CH_4 and CO_2 variations. Science 314, 285–288.
Marchal, O., Cacho, I., Stocker, T.F., Grimalt, J.O., Calvo, E., Martrat, B., Shackleton, N., Vautravers, M., Cortijo, E., van Kreveld, S., Andersson, C., Koc, N., Chapman, M., Sbaffi, L., Duplessy, J.C., Sarnthein, M., Turon, J.L., Duprat, J., Jansen, E., 2002. Apparent long-term cooling of the sea surface in the northeast Atlantic and Mediterranean during the Holocene. Quat. Sci. Rev. 21, 455–483.
Marchal, O., Stocker, T.F., Joos, F., 1998. A latitude-depth, circulation biogeochemical ocean model for paleoclimate studies. Development and sensitivities. Tellus Ser. B-Chem. Phys. Meteorol. 50, 290–316.
Marcott, S.A., Shakun, J.D., Clark, P.U., Mix, A.C., 2013. A reconstruction of regional and global temperature for the past 11,300 Years. Science 339, 1198–1201.
Marlon, J.R., Bartlein, P.J., Daniau, A.L., Harrison, S.P., Maezumi, S.Y., Power, M.J., Tinner, W., Vanniere, B., 2013. Global biomass burning: a synthesis and review of Holocene paleofire records and their controls. Quat. Sci. Rev. 65, 5–25.
Marlon, J.R., Bartlein, P.J., Gavin, D.G., Long, C.J., Anderson, R.S., Briles, C.E., Brown, K.J., Colombaroli, D., Hallett, D.J., Power, M.J., Scharf, E.A., Walsh, M.K., 2012. Long-term perspective on wildfires in the western USA. Proc. Natl. Acad. Sci. 109, E535–E543.
Menviel, L., Joos, F., 2012. Toward explaining the Holocene carbon dioxide and carbon isotope records: results from transient ocean carbon cycle-climate simulations. Paleoceanography 27.
Menviel, L., Joos, F., Ritz, S.P., 2012. Simulating atmospheric CO_2, C-13 and the marine carbon cycle during the last Glacial-Interglacial cycle: possible role for a deepening of the mean remineralization depth and an increase in the oceanic nutrient inventory. Quat. Sci. Rev. 56, 46–68.
Milliman, J.D., 1993. Production and accumulation of calcium-carbonate in the ocean - budget of a nonsteady state. Glob. Biogeochem. Cycles 7, 927–957.
Monnin, E., Steig, E.J., Siegenthaler, U., Kawamura, K., Schwander, J., Stauffer, B., et al., 2004. Evidence for substantial accumulation rate variability in Antarctica during the Holocene, through synchronization of CO2 in the Taylor Dome, Dome C and DML ice cores. Earth Planet. Sci. Lett 224 (1–2), 45–54.
Muller, S.A., Joos, F., Edwards, N.R., Stocker, T.F., 2006. Water mass distribution and ventilation time scales in a cost-efficient, three-dimensional ocean model. J. Clim. 19, 5479–5499.
Neftel, A., Oeschger, H., Schwander, J., Stauffer, B., Zumbrunn, R., 1982. Ice core sample measurements give atmospheric CO_2 content during the past 40,000 yr. Nature 295, 220–223.
New, M., Hulme, M., Jones, P., 2000. Representing twentieth-century space-time climate variability. Part II: development of 1901-96 monthly grids of terrestrial surface climate. J. Clim. 13, 2217–2238.
Olofsson, J., Hickler, T., 2008. Effects of human land-use on the global carbon cycle during the last 6,000 years. Veg. Hist. Archaeobotany 17, 605–615.
Opdyke, B.N., Walker, J.C.G., 1992. Return of the coral reef hypothesis: Basin to shelf partitioning of $CaCO_3$ and its effect on atmospheric CO_2. Geology 20, 730–736.
Parekh, P., Joos, F., Muller, S.A., 2008. A modeling assessment of the interplay between aeolian iron fluxes and iron-binding ligands in controlling carbon dioxide fluctuations during Antarctic warm events. Paleoceanography 23.
Parrenin, F., Masson-Delmotte, V., Kohler, P., Raynaud, D., Paillard, D., Schwander, J., Barbante, C., Landais, A., Wegner, A., Jouzel, J., 2013. Synchronous change of atmospheric CO_2 and Antarctic temperature during the last Deglacial warming. Science 339, 1060–1063.
Petit, J.R., Jouzel, J., Raynaud, D., Barkov, N.I., Barnola, J.M., Basile, I., Bender, M., Chappellaz, J., Davis, M., Delaygue, G., Delmotte, M., Kotlyakov, V.M., Legrand, M., Lipenkov, V.Y., Lorius, C., Pepin, L., Ritz, C., Saltzman, E., Stievenard, M., 1999. Climate and atmospheric history of the past 420,000 years from the Vostok ice core, Antarctica. Nature 399, 429–436.
Petoukhov, V., Ganopolski, A., Brovkin, V., Claussen, M., Eliseev, A., Kubatzki, C., Rahmstorf, S., 2000. CLIMBER-2: a climate system model of intermediate complexity. Part I: model description and performance for present climate. Clim. Dyn. 16, 1–17.
Pongratz, J., Reick, C.H., Raddatz, T., Claussen, M., 2009. Effects of anthropogenic land cover change on the carbon cycle of the last millennium. Glob. Biogeochem. Cycles 23.
Power, M., Mayle, F., Bartlein, P., Marlon, J., Anderson, R., Behling, H., Brown, K., Carcaillet, C., Colombaroli, D., Gavin, D., Hallett, D., Horn, S., Kennedy, L., Lane, C., Long, C., Moreno, P., Paitre, C., Robinson, G., Taylor, Z., Walsh, M., 2013. Climatic control of the biomass-burning decline in the Americas after ad 1500. The Holocene 23, 3–13.
Power, M.J., Marlon, J., Ortiz, N., Bartlein, P.J., Harrison, S.P., Mayle, F.E., Ballouche, A., Bradshaw, R.H.W., Carcaillet, C., Cordova, C., Mooney, S., Moreno, P.I., Prentice, I.C., Thonicke, K., Tinner, W., Whitlock, C., Zhang, Y., Zhao, Y., Ali, A.A., Anderson, R.S., Beer, R., Behling, H., Briles, C., Brown, K.J., Brunelle, A., Bush, M., Camill, P., Chu, G.Q., Clark, J., Colombaroli, D., Connor, S., Daniau, A.L., Daniels, M., Dodson, J., Doughty, E., Edwards, M.E., Finsinger, W., Foster, D., Frechette, J., Gaillard, M.J., Gavin, D.G., Gobet, E., Haberle, S., Hallett, D.J., Higuera, P., Hope, G., Horn, S., Inoue, J., Kaltenrieder, P., Kennedy, L., Kong, Z.C., Larsen, C., Long, C.J., Lynch, J., Lynch, E.A., McGlone, M., Meeks, S., Mensing, S., Meyer, G., Minckley, T., Mohr, J., Nelson, D.M., New, J., Newnham, R., Noti, R., Oswald, W., Pierce, J., Richard, P.J.H., Rowe, C., Goni, M.F.S., Shuman, B.N., Takahara, H., Toney, J., Turney, C., Urrego-Sanchez, D.H., Umbanhowar, C., Vandergoes, M., Vanniere, B., Vescovi, E., Walsh, M., Wang, X., Williams, N., Wilmshurst, J., Zhang, J.H., 2008. Changes in fire regimes since the last glacial Maximum: an assessment based on a global synthesis and analysis of charcoal data. Clim. Dyn. 30, 887–907.
Prentice, I.C., Jolly, D., participants, B., 2000. Mid-Holocene and glacial-maximum vegetation geography of the northern continents and Africa. J. Biogeogr. 27, 507–519.
Raddatz, T., Reick, C., Knorr, W., Kattge, J., Roeckner, E., Schnur, R., Schnitzler, K., Wetzel, P., Jungclaus, J., 2007. Will the tropical land biosphere dominate the climate-carbon cycle feedback during the twenty-first century? Clim. Dyn. 29, 565–574.
Reeburgh, W.S., 2007. Oceanic methane biogeochemistry. Chem. Rev. 107, 486–513.
Reich, P.B., Hobbie, S.E., Lee, T.D., 2014. Plant growth enhancement by elevated CO_2 eliminated by joint water and nitrogen limitation. Nat. Geosci. 7, 920–924.
Reick, C.H., Raddatz, T., Brovkin, V., Gayler, V., 2013. Representation of natural and anthropogenic land cover change in MPI-ESM. J. Adv. Model. Earth Syst. 5, 459–482.
Ridgwell, A., Hargreaves, J.C., 2007. Regulation of atmospheric CO_2 by deep-sea sediments in an Earth system model. Glob. Biogeochem. Cycles 21.
Ridgwell, A., Hargreaves, J.C., Edwards, N.R., Annan, J.D., Lenton, T.M., Marsh, R., Yool, A., Watson, A., 2007. Marine geochemical data assimilation in an efficient Earth system model of global biogeochemical cycling. Biogeosciences 4, 87–104.
Ridgwell, A.J., Watson, A.J., Maslin, M.A., Kaplan, J.O., 2003. Implications of coral reef buildup for the controls on atmospheric CO_2 since the last glacial maximum. Paleoceanography 18. http://dx.doi.org/10.1029/2003PA000893.
Ritz, S.P., Stocker, T.F., Joos, F., 2011. A coupled dynamical ocean-energy balance atmosphere model for Paleoclimate studies. J. Clim. 24, 349–375.
Roth, R., Joos, F., 2012. Model limits on the role of volcanic carbon emissions in regulating glacial-interglacial CO_2 variations. Earth Planet. Sci. Lett. 329, 141–149.
Roth, R., Ritz, S.P., Joos, F., 2014. Burial-nutrient feedbacks amplify the sensitivity of atmospheric carbon dioxide to changes in organic matter remineralisation. Earth Syst. Dyn. 5, 321–343.
Ruddiman, W.F., 2003. The anthropogenic greenhouse era began thousands of years ago. Clim. Change 61, 261–293.
Ruddiman, W.F., 2013. The Anthropocene. Annu. Rev. Earth Planet. Sci. 41, 45–68.
Saito, K., Sueyoshi, T., Marchenko, S., Romanovsky, V., Otto-Bliesner, B., Walsh, J., Bigelow, N., Hendricks, A., Yoshikawa, K., 2013. LGM permafrost distribution: how well can the latest PMIP multi-model ensembles perform reconstruction? Clim. Past. 9, 1697–1714.
Sapart, C.J., Monteil, G., Prokopiou, M., van de Wal, R.S.W., Kaplan, J.O., Sperlich, P., et al., 2012. Natural and anthropogenic variations in methane sources during the past two millennia. Nature 490 (7418), 85–88.
Schmitt, J., Schneider, R., Elsig, J., Leuenberger, D., Lourantou, A., Chappellaz, J., Köhler, P., Joos, F., Stocker, T.F., Leuenberger, M., Fischer, H., 2012. Carbon isotope constraints on the deglacial CO_2 rise from ice cores. Science 336, 711–714.
Schneck, R., Reick, C.H., Raddatz, T., 2013. Land contribution to natural CO_2 variability on time scales of centuries. J. Adv. Model. Earth Syst. 5, 354–365.
Schneider, R., Schmitt, J., Koehler, P., Joos, F., Fischer, H., 2013. A reconstruction of atmospheric carbon dioxide and its stable carbon isotopic composition from the penultimate glacial maximum to the last glacial inception. Clim. Past 9, 2507–2523.
Schurgers, G., Mikolajewicz, U., Groger, M., Maier-Reimer, E., Vizcaino, M., Winguth, A., 2006. Dynamics of the terrestrial biosphere, climate and atmospheric CO_2 concentration during interglacials: a comparison between Eemian and Holocene. Clim. Past 2, 205–220.
Schuur, E.A.G., Abbott, B.W., Bowden, W.B., Brovkin, V., Camill, P., Canadell, J.G., Chanton, J.P., Chapin III, F.S., Christensen, T.R., Ciais, P., Crosby, B.T., Czimczik, C.I., Grosse, G., Harden, J., Hayes, D.J., Hugelius, G., Jastrow, J.D., Jones, J.B., Kleinen, T., Koven, C.D., Krinner, G., Kuhry, P., Lawrence, D.M., McGuire, A.D., Natali, S.M., O'Donnell, J.A., Ping, C.L., Riley, W.J., Rinke, A., Romanovsky, V.E., Sannel, A.B.K., Schaedel, C., Schaefer, K., Sky, J., Subin, Z.M., Tarnocai, C., Turetsky, M.R., Waldrop, M.P., Anthony, K.M.W., Wickland, K.P., Wilson, C.J., Zimov, S.A., 2013.

Expert assessment of vulnerability of permafrost carbon to climate change. Clim. Change 119, 359–374.
Shakhova, N., Semiletov, I., Leifer, I., Sergienko, V., Salyuk, A., Kosmach, D., Chernykh, D., Stubbs, C., Nicolsky, D., Tumskoy, V., Gustafsson, O., 2014. Ebullition and storm-induced methane release from the East Siberian Arctic Shelf. Nat. Geosci. 7, 64–70.
Shanahan, T.M., McKay, N.P., Hughen, K.A., Overpeck, J.T., Otto-Bliesner, B., Heil, C.W., King, J., Scholz, C.A., Peck, J., 2015. The time-transgressive termination of the African Humid Period. Nat. Geosci. 8, 140–144.
Sitch, S., Smith, B., Prentice, I.C., Arneth, A., Bondeau, A., Cramer, W., Kaplan, J.O., Levis, S., Lucht, W., Sykes, M.T., Thonicke, K., Venevsky, S., 2003. Evaluation of ecosystem dynamics, plant geography and terrestrial carbon cycling in the LPJ dynamic global vegetation model. Glob. Change Biol. 9, 161–185.
Sowers, T., 2006. Late quaternary atmospheric CH_4 isotope record suggests marine clathrates are stable. Science 311, 838–840.
Sowers, T., 2010. Atmospheric methane isotope records covering the Holocene period. Quat. Sci. Rev. 29, 213–221.
Spahni, R., Joos, F., Stocker, B.D., Steinacher, M., Yu, Z.C., 2013. Transient simulations of the carbon and nitrogen dynamics in northern peatlands: from the last glacial maximum to the 21st century. Clim. Past 9, 1287–1308.
Stocker, B.D., Spahni, R., Joos, F., 2014. DYPTOP: a cost-efficient TOPMODEL implementation to simulate sub-grid spatio-temporal dynamics of global wetlands and peatlands. Geosci. Model Dev. 7, 3089–3110.
Stocker, B.D., Strassmann, K., Joos, F., 2011. Sensitivity of Holocene atmospheric CO_2 and the modern carbon budget to early human land use: analyses with a process-based model. Biogeosciences 8, 69–88.
Strassmann, K.M., Joos, F., Fischer, G., 2008. Simulating effects of land use changes on carbon fluxes: past contributions to atmospheric CO_2 increases and future commitments due to losses of terrestrial sink capacity. Tellus Ser. B-Chemical Phys. Meteorol. 60, 583–603.
Tarasov, P.E., Andreev, A.A., Anderson, P.M., Lozhkin, A.V., Leipe, C., Haltia, E., Nowaczyk, N.R., Wennrich, V., Brigham-Grette, J., Melles, M., 2013. A pollen-based biome reconstruction over the last 3.562 million years in the far East Russian Arctic - new insights into climate-vegetation relationships at the regional scale. Clim. Past 9, 2759–2775.
Tarnocai, C., Canadell, J.G., Schuur, E.A.G., Kuhry, P., Mazhitova, G., Zimov, S., 2009. Soil organic carbon pools in the northern circumpolar permafrost region. Glob. Biogeochem. Cycles 23.
Tschumi, T., Joos, F., Gehlen, M., Heinze, C., 2011. Deep ocean ventilation, carbon isotopes, marine sedimentation and the deglacial CO_2 rise. Clim. Past 7, 771–800.
Tschumi, T., Joos, F., Parekh, P., 2008. How important are Southern Hemisphere wind changes for low glacial carbon dioxide? A model study. Paleoceanography 23, PA4208.
Tzedakis, P.C., Wolff, E.W., Skinner, L.C., Brovkin, V., Hodell, D.A., McManus, J.F., Raynaud, D., 2012. Can we predict the duration of an interglacial? Clim. Past 8, 1473–1485.
van Nes, E.H., Scheffer, M., Brovkin, V., Lenton, T.M., Ye, H., Deyle, E., Sugihara, G., 2015. Causal feedbacks in climate change. Nat. Clim. Change 5, 445–448.
Vecsei, A., Berger, W.H., 2004. Increase of atmospheric CO_2 during deglaciation: constraints on the coral reef hypothesis from patterns of deposition. Glob. Biogeochem. Cycles 18.
Volk, T., Hoffert, M.I., 1985. Ocean carbon pumps: analysis of relative strengths and efficiencies in ocean driven atmospheric CO_2 changes. In: Sundquist, E.T., Broecker, W.S. (Eds.), The Carbon Cycle and Atmospheric CO_2: Natural Variations Archaean to Present, Geophys. Monogr. Ser.. AGU, Washington, D.C., pp. 99–110
Walker, A.P., Zaehle, S., Medlyn, B.E., De Kauwe, M.G., Asao, S., Hickler, T., Parton, W., Ricciuto, D.M., Wang, Y.P., Warlind, D., Norby, R.J., 2015. Predicting long-term carbon sequestration in response to CO_2 enrichment: how and why do current ecosystem models differ? Glob. Biogeochem. Cycles 29, 476–495.
Wang, Z., Chappellaz, J., Park, K., Mak, J.E., 2010. Large variations in Southern Hemisphere biomass burning during the last 650 Years. Science 330, 1663–1666.
Williams, J.W., 2003. Variations in tree cover in North America since the last glacial maximum. Glob. Planet. Change 35, 1–23.
Wirtz, K.W., Lemmen, C., 2003. A global dynamic model for the neolithic transition. Clim. Change 59, 333–367.
Yang, X.Y., Barton, H.J., Wan, Z.W., Li, Q., Ma, Z.K., Li, M.Q., Zhang, D., Wei, J., 2013. Sago-type palms were an important plant food prior to Rice in Southern Subtropical China. Plos One 8.
Yu, J.M., Broecker, W.S., Elderfield, H., Jin, Z.D., McManus, J., Zhang, F., 2010a. Loss of carbon from the deep sea since the last glacial maximum. Science 330, 1084–1087.
Yu, Z.C., 2012. Northern peatland carbon stocks and dynamics: a review. Biogeosciences 9, 4071–4085.
Yu, Z.C., Loisel, J., Brosseau, D.P., Beilman, D.W., Hunt, S.J., 2010b. Global peatland dynamics since the last glacial Maximum. Geophys. Res. Lett. 37.
Zaehle, S., 2013. Terrestrial nitrogen - carbon cycle interactions at the global scale. Philos. Trans. R. Soc. B-Biol. Sci. 368.
Zennaro, P., Kehrwald, N., Marlon, J., Ruddiman, W., Brücher, T., Agostinelli, C., Dahl-Jensen, D., Zangrando, R., Gambaro, A., Barbante, C., 2015. Europe on fire three thousand years ago: Arson or climate? Geophys. Res. Lett. 42, 5023–2033.
Zennaro, P., Kehrwald, N., McConnell, J.R., Schupbach, S., Maselli, O.J., Marlon, J., Vallelonga, P., Leuenberger, D., Zangrando, R., Spolaor, A., Borrotti, M., Barbaro, E., Gambaro, A., Barbante, C., 2014. Fire in ice: two millennia of boreal forest fire history from the Greenland NEEM ice core. Clim. Past 10, 1905–1924.